Journal of
Manufacturing and Materials Processing

MDPI

Article

Procedure for Reconstruction, Modeling, and Fabrication Using Additive and Rapid Tooling Methods of a Training Model for Transsphenoidal Surgery

Giacomo Santona [1], Antonio Fiorentino [2,*], Francesco Doglietto [3,4] and Mauro Serpelloni [1]

[1] Department of Information Engineering, University of Brescia, 25123 Brescia, Italy; giacomo.santona@unibs.it (G.S.); mauro.serpelloni@unibs.it (M.S.)
[2] Department of Mechanical and Industrial Engineering, University of Brescia, 25123 Brescia, Italy
[3] Neurosurgery, Department of Neurosciences, Sensory Organs and Thorax, Università Cattolica del Sacro Cuore, 00168 Rome, Italy; francesco.doglietto@unicatt.it
[4] Neurosurgery, Fondazione Policlinico Universitario A. Gemelli IRCCS, 00136 Rome, Italy
* Correspondence: antonio.fiorentino@unibs.it

Abstract: The endoscopic transsphenoidal approach (ETA) is a novel approach used by neurosurgeons and otolaryngologists to treat pituitary adenoma, and it has a long learning curve. Training is mostly performed using cadaver heads, but their low availability and cost can limit their use. ETA training models can be used to overcome these limitations. In this panorama, additive manufacturing (AM) technologies represent a more flexible and cost-effective solution to fabricate custom-made training models. Their development involves computed tomography (CT) segmentation, STL file elaboration, direct 3D printing, and rapid parts tooling. This work presents and discusses the entire procedure applied to a modular ETA training model. The procedure starts with selecting the material and AM processes based on a literature review. Accordingly, the parts of the model were designed, 3D printed, or rapid cast. In particular, fused filament fabrication (FFF) was adopted for those tissues whose materials could be directly printed (bones and cartilage), while the rapid casting of silicone was adopted for soft tissues (skin and mucosa) together with FFF to fabricate mold patterns and cores. After fabrication and assembly, the model was finally tested by an experienced neurosurgeon who provided feedback. Moreover, the cost and time of the prototype fabrication were assessed. Results validated the proposed solution from both the surgical and commercial points of view. Moreover, general procedures for designing and rapidly fabricating ETA models were generalized to make them exploitable to more general case studies.

Keywords: additive manufacturing; rapid tooling; rapid casting; transsphenoidal surgery; training model

Academic Editor: Sharifu Ura

Received: 24 December 2024
Revised: 3 February 2025
Accepted: 6 February 2025
Published: 18 February 2025

Citation: Santona, G.; Fiorentino, A.; Doglietto, F.; Serpelloni, M. Procedure for Reconstruction, Modeling, and Fabrication Using Additive and Rapid Tooling Methods of a Training Model for Transsphenoidal Surgery. *J. Manuf. Mater. Process.* **2025**, *9*, 63. https://doi.org/10.3390/jmmp9020063

1. Introduction

The pituitary gland is located below the hypothalamus in the sella turcica, a saddle-shaped prominence on the back of the sphenoid bone. The sellar region is also the location of the arachnoid membrane, the optic chiasm, and the internal carotid artery. A tumor can grow on the pituitary gland, resulting in an alteration to the functioning of the gland. Such a tumor is called pituitary adenoma or Pituitary Neuro-Endocrine Tumor (PA or PitNET), and its optimal surgical treatment requires years of experience in the field [1–4]. Nowadays, one novel surgical technique to treat PAs is the endoscopic transsphenoidal approach (ETA). ETA surgery consists of removing the PA by entering through the nostril

cavities with the instruments. Then, the sphenoid sinus is opened to expose and remove the PA. The surgery is usually performed by both neurosurgeons and otolaryngologists and requires experience, high skills, and great hand–eye coordination. Nowadays, surgeons, to overcome the significant learning curve of ETA, can acquire experience in the field or by training in the anatomical labs with cadaver heads [2,3], which is still the gold standard in terms of training and advanced skills acquisition [1]. However, training with cadaver heads is not always an accessible solution due to their low availability and their high costs. Moreover, clinical anatomy or disease depends on the donor, and the surgeon cannot decide a priori which case to train on.

With the recent improvements and accessibility of additive manufacturing (AM) technologies, the application of AM in the field of medicine has gradually developed over time [5]. This is leading to the development of new alternatives to classical surgical training allowing the fabrication of realistic anatomical models [1,5]. The main reason is the possibility of obtaining complex anatomical geometries at relatively low costs [6,7].

For these reasons, the present research focuses on the development of a training model for ETA, from the CT of a patient to the fabrication of the model. In particular, the paper presents, discusses, and validates a comprehensive procedure developed for its design and rapid fabrication.

This research starts with literature and market reviews to outline the current solutions and products, evaluating which materials are used to emulate the tissues of interest, how they are processed, and the prices of commercial products. Based on the results, a flexible and cost-effective solution that guarantees the replication of the tissue behaviors (suitable for bones, cartilage, mucosa, and skin) and additive manufacturability is outlined. Then, the paper proposes the procedure adopted to design the ETA model by isolating anatomical details, coupling parts, and designing molds and cores. Finally, it describes the direct manufacturing of the parts using fused filament fabrication (FFF) of polylactic acid (PLA) and thermoplastic polyurethane (TPU) and, in particular, the silicone rapid casting process.

The fabricated ETA model was then validated. In particular, a team of surgeons furnished their positive feedback together with suggestions for enhancing the product. Moreover, cost and time estimations demonstrated that the product is market-consistent and can be competitive.

Overall, the article contains complete and detailed information collected and processed to be exploitable in other applications, regardless of the case study presented. In particular, research on materials and technologies reports a long list of possible alternatives that can be explored or implemented where required. Furthermore, the design and rapid casting procedures for fabricating training models are generalized, and procedural details are provided to make them exploitable for other case studies. Finally, market prospects represent a reference for verifying and allocating similar products.

2. Selection of Materials and Processes

Research on materials, production technologies, and commercial products was performed considering the solutions present in the literature and on the market. The tissues of interest for the development of the ETA training model are the bone (i.e., the sphenoid bone), cartilage (i.e., nasal septum), skin (i.e., the nose), the mucosa (turbinates), the dura mater, the arachnoid membrane, and the pituitary tumor. Results are reported in Tables 1–3. Table 1 reports the information focused on the replication of the tissue's general behaviors, independently from the application. Table 2 collects the results correlated to the fabrication of ETA models, including their price. Finally, Table 3 reports the prices of other commercial products for which the manufacturing details were not declared.

The information collected on materials and additive manufacturing processes (Tables 1 and 2) was used to design the manufacturing process of the modules of the ETA model. In particular, the choice was made preferring those solutions characterized by the capability of emulating the mechanical and haptic properties of biological tissues involved, a higher flexibility in terms of materials, and a lower cost. Accordingly, the FFF process was selected for the fabrication of rigid parts and tools. In particular, the nasal septum was 3D printed in TPU, whose lower flexural modulus compared to PLA is more suitable for imitating cartilaginous tissues [8], and PLA was selected to replicate bone tissues [9–13]. Moreover, the mechanical properties of the nose and turbinate, respectively made of skin and mucosa, are well replicated by silicone [14–19]. Given the complexity of the 3D printing of silicone [20], rapid tooling was chosen to fabricate silicone modules [7,21]. Furthermore, silicone rapid casting allows one to choose amongst a wide range of material hardness for replicating soft tissues compared to commercial feedstock materials of selective laser sintering (SLS) [22] or PolyJet (PJ) [23].

Table 1. The materials and production technologies used to reproduce the different modules of biological tissues.

Tissue	Material	Production Technology	References
Bone	PLA	FFF/FDM	[9–13]
	PA with glass beads	SLS	[24–26]
	CAH	BJ	[27,28]
	3DPIC	BJ and Mold Casting	[29]
Cartilage	TPU	FFF	[8]
Skin	Silicone	Mold Casting	[14,16,17]
	Agar	-	[14]
	Gelatin	-	[14]
	Polyurethane	-	[14,30]
	PVA	-	[14]
Mucosa	Silicone	Mold Casting	[15]
Dura Mater	Silicone	Coating	[24,26,31,32]
	Polyurethane	Coating	[28]
Arachnoid	Polymeric film	-	[33,34]
Tumor	Resin [a]	-	[2,35]
	Boiled Egg	-	[22,23,36]
	Agar	Mold Casting	[37]

Abbreviation: FFF = fused filament fabrication, FDM = fused deposition modeling, SLA = stereolithography, SLS = selective laser sintering, BJ = binder jetting, PLA = polylactic acid, CAH = cyanoacrylate with hydroquinone, 3DPIC = 3D polymer-infiltrated composite, ST-504, PVA = polyvinyl alcohol, TPU = thermoplastic polyurethane. [a] = Stratathane ST-504 Vari-Lok injection resin.

Table 2. Materials, production technologies, 3D printers, and the price of commercial ETA models [1].

Tissue/Anatomy	Material	Technology	3D Printer	Costs	Ref.
Head	n/d	PJ	Connex 500	n/a	[38]
Rigid Components [d]	Duraform PA12	SLS	DTM Sinterstation 2500 plus	2500 EUR	[22]
Flexible Components [d]	Duraform Flex	SLS	EOS P760		
Sellar region	Thermosetting resin impregnated with polyester resin	MJ	ProJet® 160	200 USD [a]	[18]
Brain, Dura Mater and Pituitary Tumor	Silicone Rubber	RC	-		
Nose	Silicone Rubber ProtoFlex 150-05	RC	-		
Head	n/d	PJ	Objet750 Connex	500 USD [b]	[39]
Head	VeroCyan, VeroMajenta and VeroYellow	PJ	Connex3 Objet350	n/a	[34]
Skin, turbinate, ICA and optic chiasm	Soft material [d]	PJ	J750	n/a	[23]
Bones	Hard material [d]				
Head	n/d	PJ	Objet J750 Connex	n/a	[40]
Skull	PLA	FFF	Ultimaker2	n/a	[15]
Surgical Area [d]	Plaster	BJ	ProJet 660 Pro		
Face, ICA, pituitary g land and optic nerves	Silicone	RC	-		
Head	VisiJet PXL powder	CJP	-	63 USD [a]	[41]
Internal nasal anatomy	n/d	SLA	Form 2	80 USD [c]	[19]
Soft tissues	Silicone	RC	-		

Abbreviations: BJ = binder jetting, CJP = ColorJet printing process, FFF = fused filament fabrication, ICA = internal carotid artery, MJ = material jetting, PJ = PolyJet, RC = rapid casting, SLS = selective laser sintering, SLA = stereolithography, n/d = not declared, n/a = not available. [a] = cost per model, [b] = production cost, [c] = material cost, [d] = not specified.

Table 3. Commercially available models and prices [1].

Developer	Simulated Surgical Task	Price	Ref.
Pro Delphus (Olinda, PE, Brazil)	Neurosurgical Training	3.798 ÷ 1.630 USD	[24–44]
JMC (Chuo-ku, Tokyo, Japan)	Neurosurgical Training	n/a	[45–49]
Phacon GmbH (Leipzig, Germany)	Neurosurgical Training	1.870 ÷ 11.070 EUR	[50–55]
UpSurgeOn S.r.l. (Assago, MI, Italy)	Transsphenoidal Approach	600 ÷ 700 EUR	[56–59]

Abbreviations: n/a = not available.

2.1. Bone—Sphenoid Bone and Ethmoid Bone

To reproduce the sphenoid bone, polylactic acid (PLA) was chosen. Parts were fabricated by FFF technology on the Ultimaker 3 extended (Ultimaker, Utrecht, The Netherlands), using the Pearl-White PLA by Ultimaker, whose main properties, taken from its technical datasheet [60], are reported in Table 4.

2.2. Cartilage—Nasal Septum

The lower bending resistance of thermoplastic polyurethane (TPU) makes it more suitable for reproducing the flexibility of cartilaginous tissues, as reported in the literature [8]. TPU has a lower flexural modulus and a higher resistance to strain compared to PLA, making TPU more suitable than PLA for this application. Similarly, the nasal septum was fabricated using FFF technology on the Ultimaker 3 extended using the TPU 95A by Ultimaker, whose main properties, taken from its datasheet [61], are reported in Table 4.

2.3. Skin and Mucosa—Nose and Turbinates

Silicone was chosen to replicate both the nose module and the turbinates module. In particular, it was carried out using the Dragon Skin™ 30 (Smooth-O Inc., Macungie, PA, USA), whose main properties are reported in Table 4 using information from its datasheet [62]. In particular, silicone modules were produced with the traditional mold casting technology, since the additive manufacturing process of two-component silicone is not mature yet [20]. The skin and mucosa silicone molds were fabricated using PLA print cores of the parts into which the silicone was poured. The fabrication of silicone components is described in the following sections.

Table 4. Mechanical properties of Pearl-White PLA and TPU 95A. XY, YZ, and Z refer to the orientation of the specimen tested; XY is the printing plate, while Z is the printing direction. Data are taken from material datasheets [60–62]. NB = no break (>10%).

Mechanical Property	Material	Value (Orientation)		
		(XY—Flat)	(YZ—Side)	(Z—Up)
Flexural modulus (MPa)	PLA	3019 ± 87	2894 ± 53	2740 ± 47
Flexural strain at break (%)		4.8 ± 0.2	NB	1.9 ± 0.2
Hardness (Shore D scale)			84	
Flexural modulus (MPa)	TPU 95A	62.6 ± 1.7	55.1 ± 2.4	62.6 ± 2.0
Flexural strain at break (%)		NB	NB	NB
Hardness (Shore D scale)			48	
Hardness (Shore A scale)	Silicone		30	
Pot life			45 min	
Curing time			16 h	

2.4. Dura Mater, Arachnoid, and Tumor

The arachnoid membrane was reproduced with the polymeric food film as found in the literature [33,34], which was considered a good representation in our previous work [63]. The pituitary tumor, as it was found in our systematic review [1], was reproduced following an interesting training model, called "Egghead" [22], where the sellar region and its content were reproduced using an egg [22,23,36,64–66], in particular, both the boiled yolk [22] and the boiled albumen [23,64] were used as a reproduction of the tumor. Together with the experienced surgeon, we evaluated that the boiled albumen is a good approximation and low-cost solution to mimic the mechanical properties of the pituitary tumor [67,68].

The materials suitable for the ETA model and the AM fabrication processes were accordingly selected to fabricate the parts or their tools (pattern and cores) in case of a rapid casting process. Table 5 reports an overview of the selected materials and AM processes together with the tissues to be manufactured and the hierarchy of the model (groups and modules) that will be further described.

Table 5. Module of the training model, the fabrication technologies, and the materials used for their production.

Group	Module	Tissue	Process	AM		RC	Disp.
				Material	Technology	Material	
Face	Face	Skin	RC	PLA	FFF (Pattern)	Silicone	no
	Ethmoid bone	Cortical Bone	AM	PLA	FFF	-	no
	Nostril (core)	Cavity	RC	PLA	FFF (Core)	-	no
Nose	Nasal septum	Cartilage	AM	TPU 95A	FFF	-	yes
Nasal cavity	Turbinates	Mucosa	RC	PLA	FFF (Pattern)	Silicone	yes
	Frame	Non-anatomical	AM	PLA	FFF	-	no
Skull base	Sphenoid bone	Cortical Bone	AM	PLA	FFF	-	yes
	Ethmoid bone	Cortical Bone	AM	PLA	FFF	-	no
	Arachnoid	Arachnoid membrane	-	Polymeric food film	-	-	yes
	Tumor	Pituitary adenoma	-	Egg white	-	-	yes

Abbreviations: AM = additive manufacturing, RC = rapid casting, Disp. = disposable.

3. Design of the Model

The flowchart of the design process is reported in Figure 1 with the main steps of the procedure and the hierarchy of the parts of the ETA model. The anatomy was obtained from a CT scan using a 1 × 1 frame with contiguous slices at 1.5 mm and a gantry angle of 0°. The scan window was 225 mm in diameter and used a pixel size of 0.44 mm. The CT scan was segmented using Materialize Mimics© software v22.0 and converted to STL format files. Then, Meshmixer (Autodesk Inc., San Francisco, CA, USA) was used to edit the STL file. In particular, the initial editing consists of general cleaning of the mesh by eliminating the errors on the STL file (mostly removal of isolated parts and repairing holes and open edges in the mesh, using the *Inspector* tool). Then, the area of interest is cropped (Figure 2), initially divided into sub-parts (Figure 3) that will be used to then design the three main groups (Figure 4): Face (from Figure 2a with the ethmoid bone in Figure 3a), Nasal Cavity (from Figure 3b), and Skull Base (from the sphenoid bone in Figure 3a). Each part was isolated using the *Plane Cut* tool and locally fixed using the *Inspector* and *Sculp* tools to remove any not useful cavities inside the bones or to fix small mesh errors. Finally, the modules were edited as described below until the final ETA model was obtained (Figure 4).

3.1. The Face Group

The Face group (Figure 4) consists of the face (Figure 2a) and a section of the ethmoid bone (Figure 3a). Nostril cavities are included to allow access for surgical instruments in the training model. The face is made by rapid casting using the ethmoid bone and nostril cores 3D printed in PLA as mold inserts. In addition, the face, combined with the ethmoid and the nostril cores, was designed to become a unique casting part, where the ethmoid is embedded in silicone and the nostril cores are removed after the silicone self-cures to form the silicone mold.

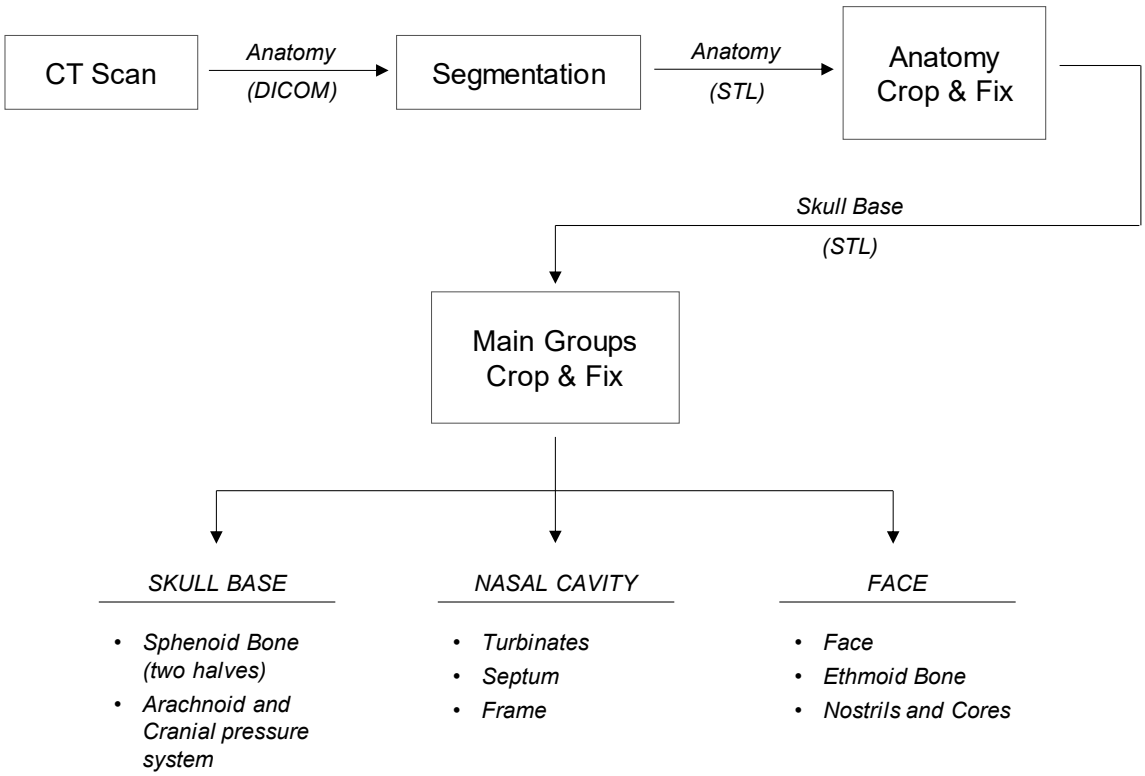

Figure 1. Designs of the ETA model—main steps and hierarchy of its components.

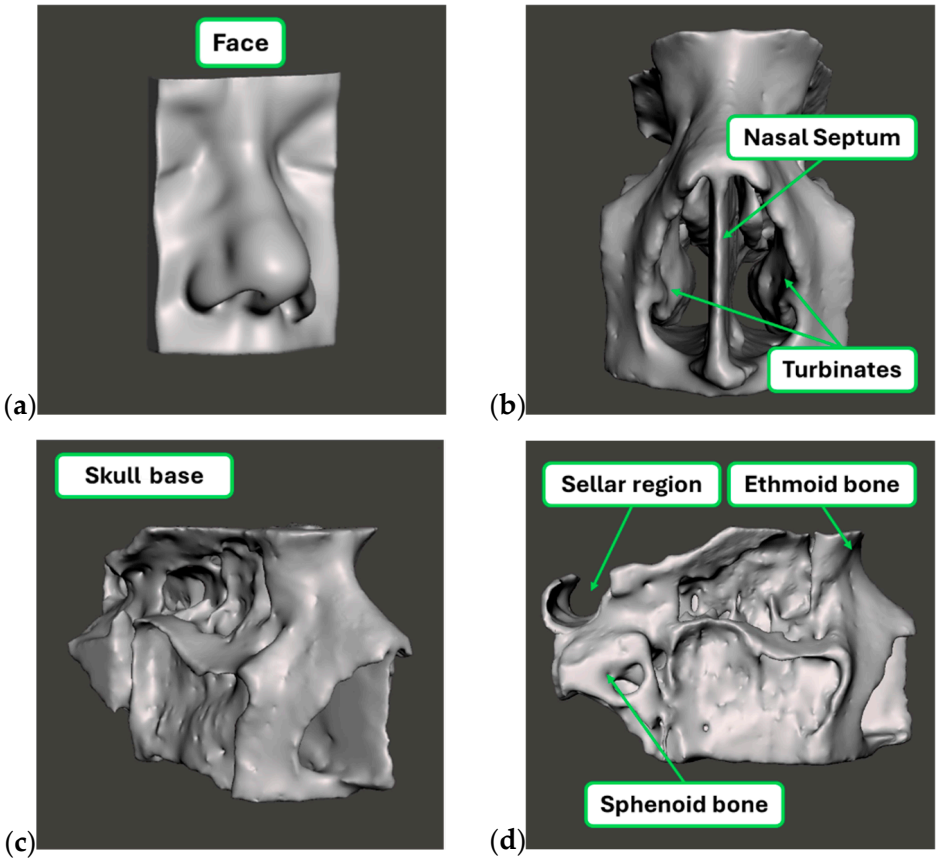

Figure 2. Anatomy of the model—initial crop from the STL file. Anatomy of (**a**) face with (**b**) frontal view of the ethmoid bone with nasal septum and turbinates, (**c**) overall skull base and (**d**) lateral view of the skull base with sellar region, sphenoid and ethmoid bones.

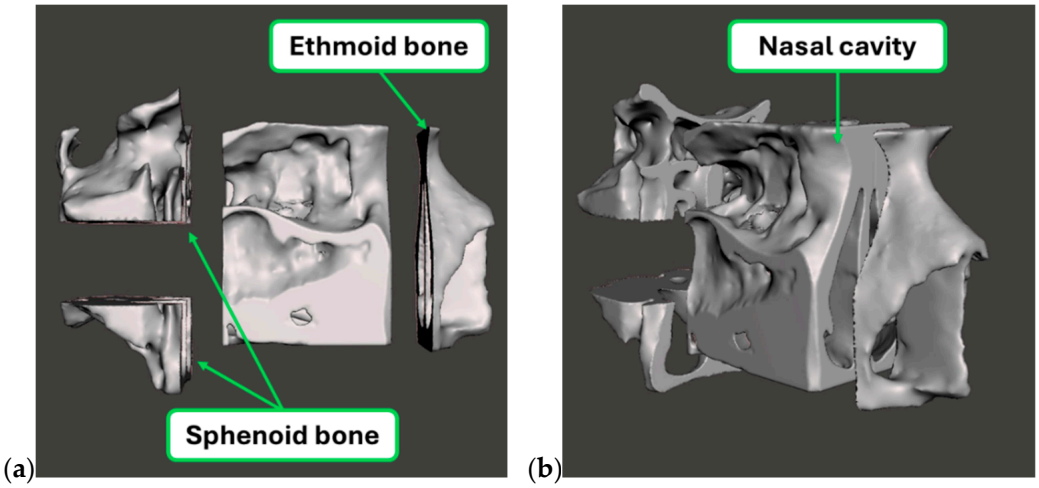

Figure 3. Examples of isolation of the anatomical modules of interest. (**a**) The ethmoid and sphenoid bones and (**b**) the nasal cavity.

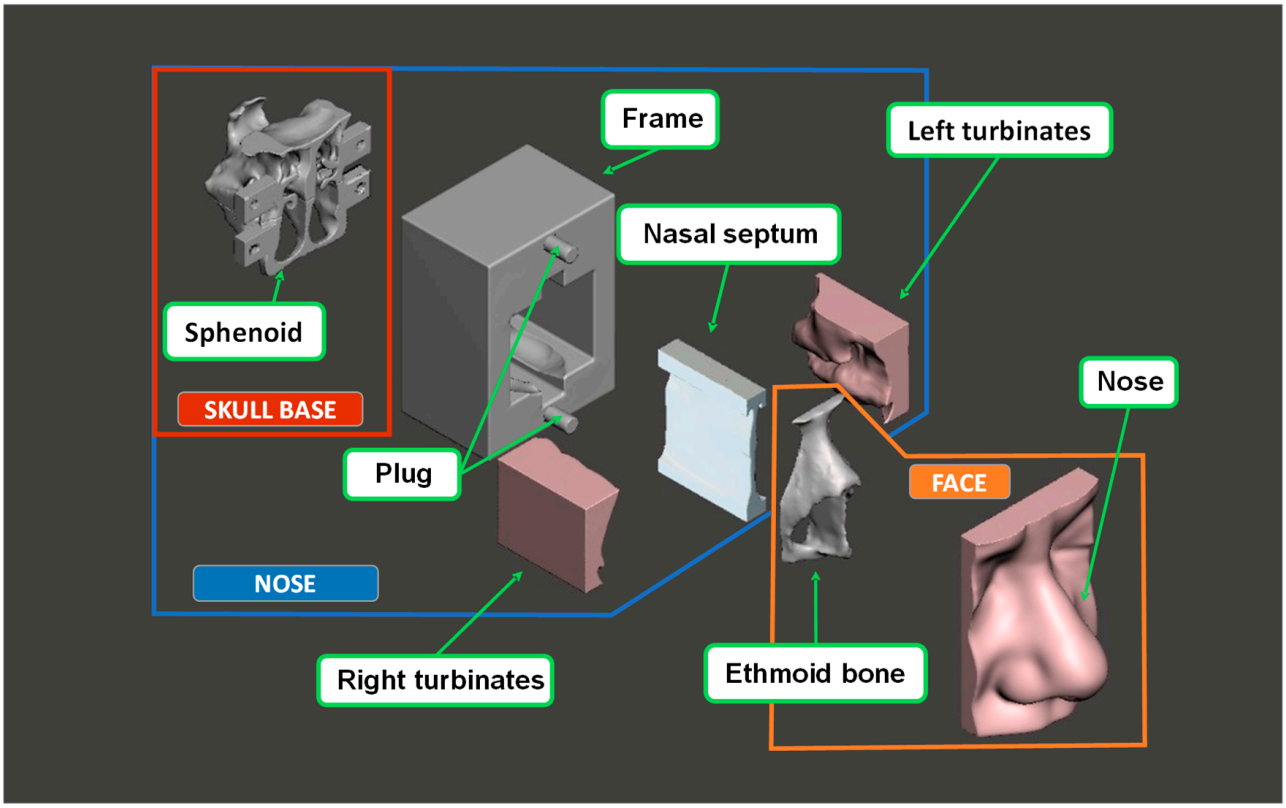

Figure 4. Exploded view of the CT-based training model with the modules highlighted.

3.1.1. Face

The face module was obtained from the head of the patient and required minor editing steps compared to the other modules. The geometry was isolated (*Plane Cut* tool), and then it was turned into a solid (*Make Solid* tool, Figure 5).

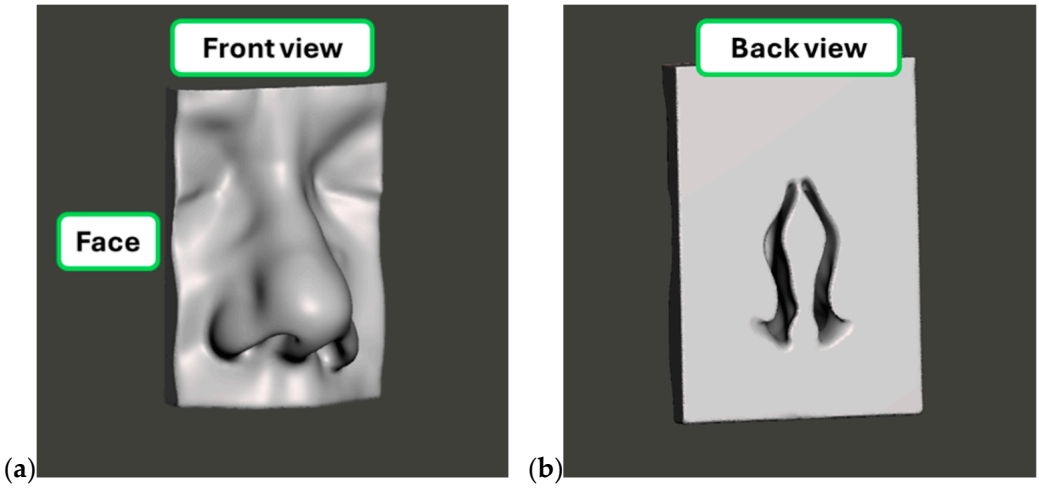

(**a**) (**b**)

Figure 5. Face module, front (**a**) and back (**b**) view.

3.1.2. Ethmoid Bone

The function of the ethmoid bone module (Figure 6) is to provide rigidity to the nose, which is better described in the following section. It was obtained using the *Plane Cut* tool from the skull base (Figure 3).

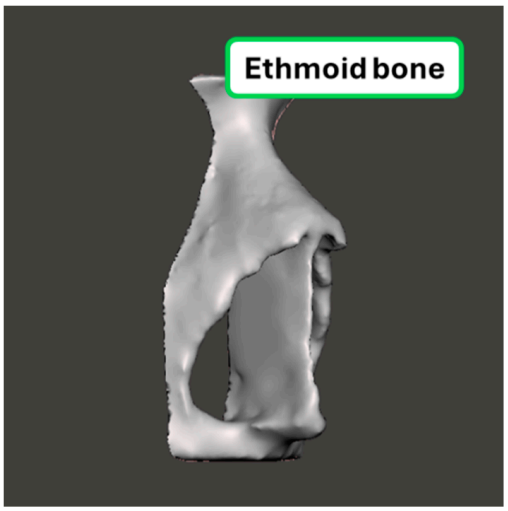

Figure 6. Ethmoid bone module.

3.1.3. Nostrils and Cores

The ETA procedure starts with surgeons inserting instruments from the nose. Therefore, reproducing the nostril cavities during the molding process is fundamental for obtaining a fully functional training model. Accordingly, two removable casting cores together with core prints were designed to reproduce the nostril cavities. Their geometry was obtained as the complementary volume of the nostril cavities to be reproduced. In particular, the edge of each cavity was manually selected using the *Select* tool (Figure 7a), and the selection boundaries were smoothed using the *Smooth Boundaries* tool to enhance the mesh (Figure 7b–d). Then, a new group was generated from the selected elements using the *Create FaceGroup* tool. The mesh was duplicated, and the elements outside the nostrils were deleted, isolating the surfaces of the nostril cavities. The obtained geometries are tubular surfaces with open ends. Therefore, they were closed using the *Auto Repair* tool with the *Flat Fill* option of the *Inspector tool,* under the *Analysis* menu (Figure 7e,f), which automatically recognizes the open surfaces and fixes the errors found (in this case, it filled the open areas).

These surfaces will become the external mesh of the cores (i.e., the complementary volume of the cavities); therefore, their normals were inverted using the *Flip Normals* tool under the *Select* menu (Figure 7g). Moreover, the use of the *Flat Fill* option allows you to obtain a smooth end surface with a low curvature. Finally, to guarantee the correct positioning of the cores in the mold, the two end surfaces of each core were selected (*Select* tool) and extruded along the Normal direction (*Extrude* tool, under the *Select* menu) to obtain the core prints (Figure 7h). Figure 7i shows the nostril cores with the core prints.

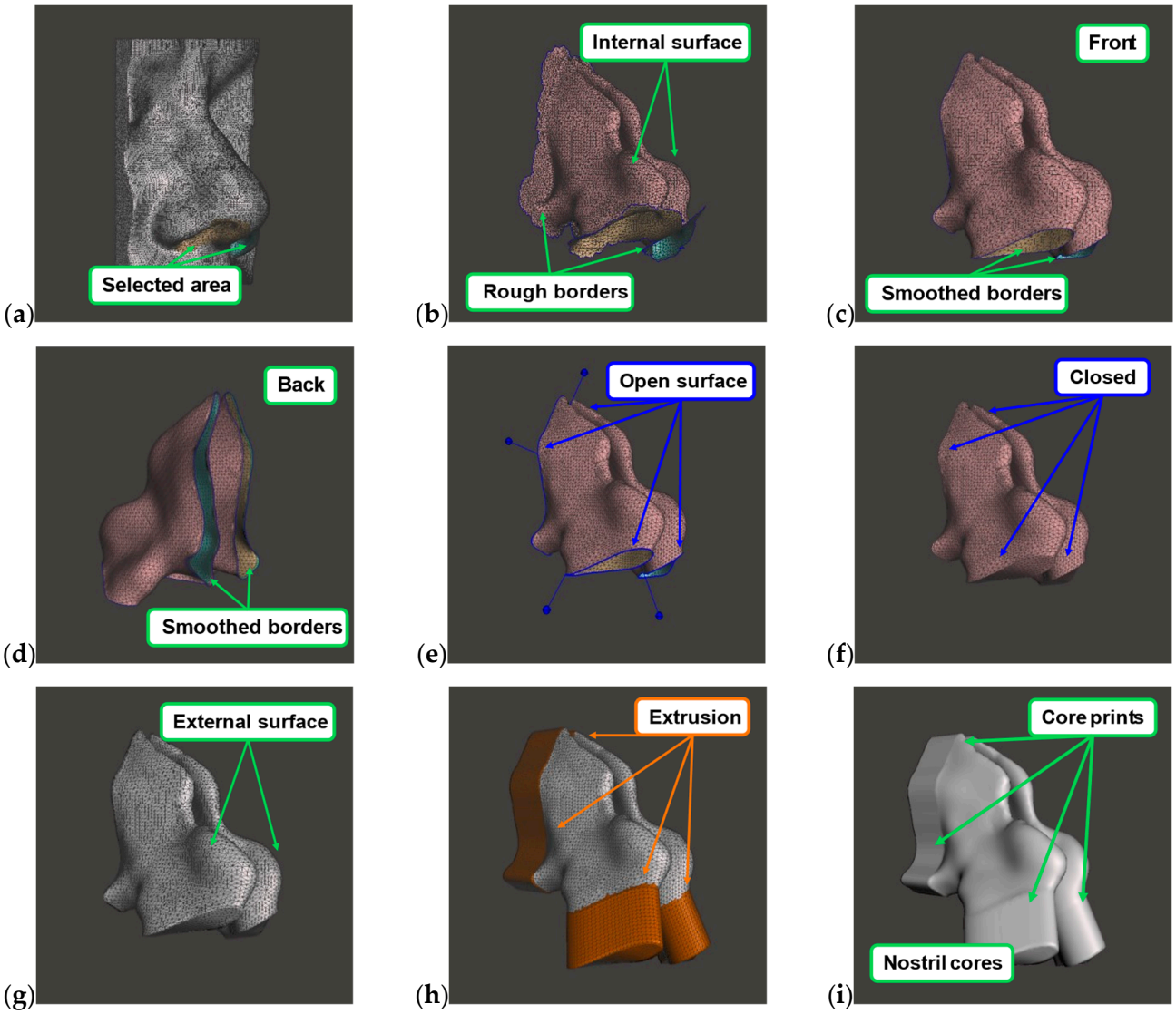

Figure 7. The edge of each cavity is manually selected using the *Select* tool and the selection boundaries are smoothed using the *Smooth Boundaries* tool to enhance the mesh quality (**a**–**d**). Then, a new group was generated from the selected elements using the *Create FaceGroup* tool. The mesh is closed using the *Inspector* tool (**e**,**f**). The mesh normals are inverted using the *Flip Normals* tool, under the *Select* menu (**g**). Moreover, the use of the *Flat Fill* option allows you to obtain a smooth end surface with a low curvature. Finally, to guarantee the correct positioning of the cores in the mold, the two end surfaces of each core were selected (*Select* tool) and extruded along the Normal direction (*Extrude* tool, under *Select* menu) to obtain the core prints (**h**). The final result: nostril cores with the core prints (**i**).

After casting, the cores will be extracted from both the silicone and the ethmoid bone once the silicone used for the face model has been cured. Before pouring the face silicone, the nostrils are inserted into the ethmoid bone, as shown in Figure 8, and then they are inserted into the silicone mold. Moreover, there must be no interference between cores and ethmoid modules, especially in the core prints. In fact, the manual and automatic tools used to design them may introduce minor geometrical errors that do not necessarily meet the anatomy of the patient. Accordingly, the presence of geometrical interferences can be verified by overlapping the ethmoid bone module with the two nostrils module as shown in Figure 9a. The overlapping volume was removed from the ethmoid bone module using the *Boolean Difference* tool, under the *Edit* menu, which is clear by comparing the ethmoid bone before (Figure 9b) and after (Figure 9c) the Boolean difference. Figure 9d shows the nostrils inserted into the ethmoid bone with no overlapping volume.

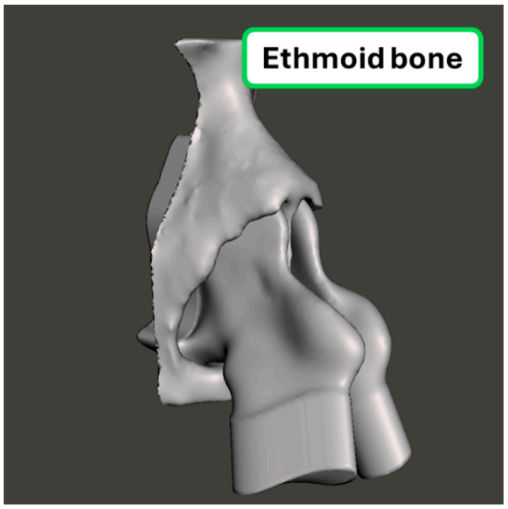

Figure 8. Ethmoid bone with nostril cores fitted within.

Once the face, cores, and ethmoid bone are designed, the pattern required to prepare the silicone molds can be designed (Figure 10). In particular, the pattern is obtained by the union of face and core modules. This was achieved by joining the meshes of the modules using the *Combine* tool and then transforming them into a single part using the *Make Solid* tool, which is the final geometry of the pattern. Additionally, two holes were added to the back of the nose module using the *Boolean Difference* tool with a cylinder (Figure 10b). The holes will be used to connect, using two cylindrical plugs, the face module with the frame, as shown in Figure 4.

3.2. The Nasal Cavity Group

The Nasal Cavity group represents the passage from the nostrils to the sphenoid bone during the ETA procedure. Moreover, from the assembly point of view, it connects the Face and Skull Base groups (Figure 3). Given the geometrical complexity of the nasal cavity (Figure 11a,b), a frame was designed around the anatomical modules to improve the "assemblability" of the model. Accordingly, several parallelepipeds were added and merged into a single object (*Combine* tool, Figure 11c, followed by the *Make Solid* tool, Figure 11d). The parallelepipeds formed closed holes around the original anatomy (Figure 11e) that were removed (*Select* tool on surfaces to preserve, followed by *Invert* and *Discard*) thus obtaining the final geometry of the entire nasal cavity (Figure 11f).

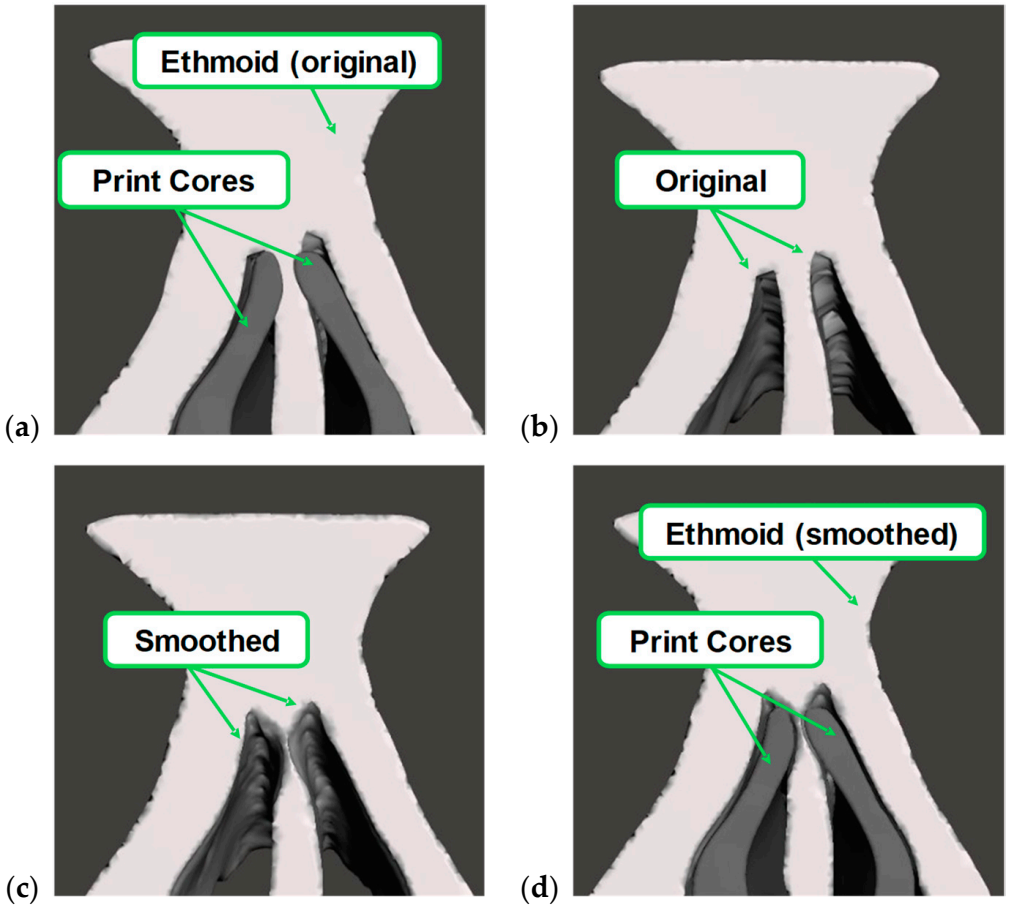

Figure 9. The nostril core overlapped on the ethmoid bone (**a**,**d**). Before and after the Boolean difference and between the ethmoid bone and the nostril cores (**b**,**c**). The nostril cores are inserted in the ethmoid bone with no overlapping volume.

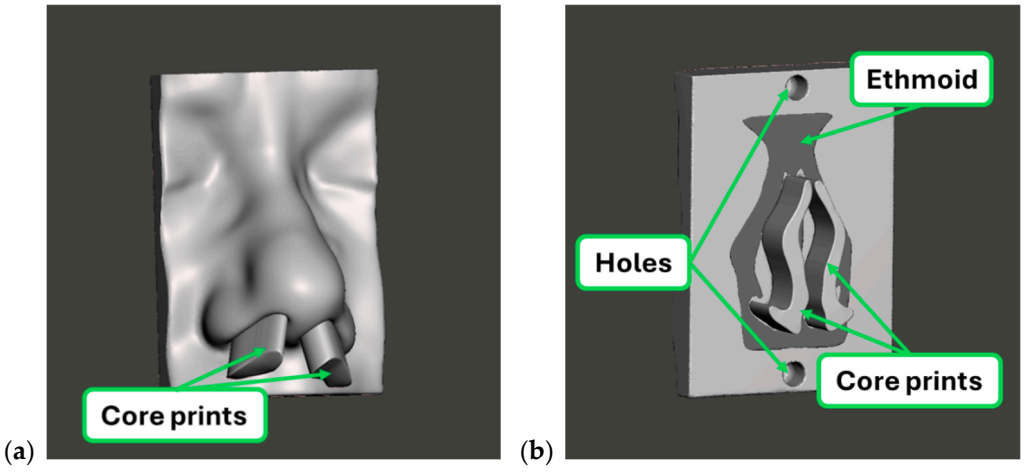

Figure 10. Pattern for the Face mold. Nose module with the core prints and the ethmoid bone inserted within. Two holes were added to allow the connection of the nose module to the frame module with two cylindrical plugs. Front (**a**) and back (**b**) view.

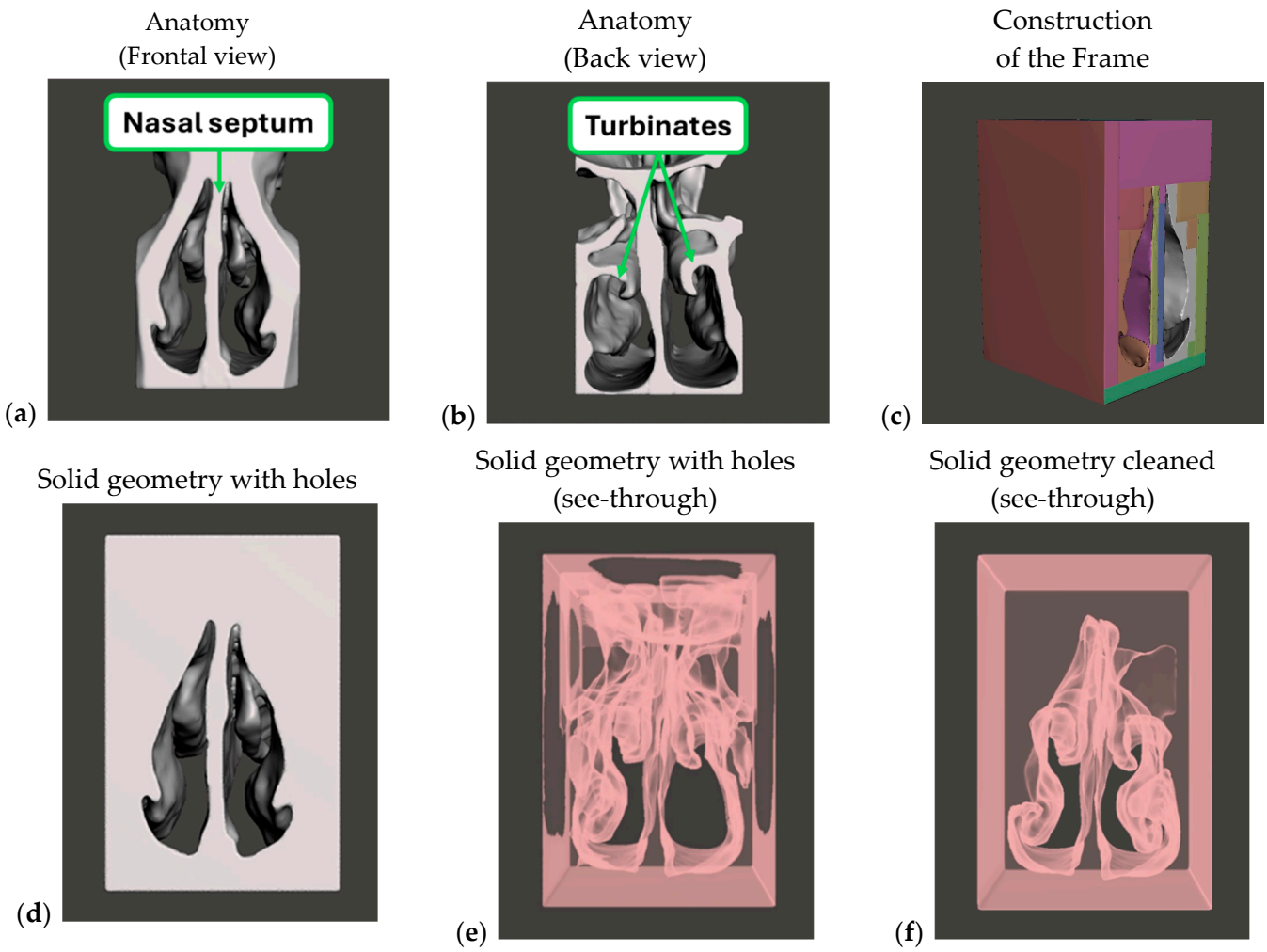

Figure 11. The design procedure of the Nasal Cavity group. It is derived from the anatomy of (**a**) the nasal septum and (**b**) turbinates. Then, (**c**) the frame was obtained with several parallelepipeds that were merged and converted into a (**d**) solid geometry with (**e**) inner cavity defects. The (**f**) final geometry of the entire Nasal Cavity group was obtained after removing the cavities.

Then, the entire nasal cavity was finally divided into three modules that form the Nasal Cavity group: Turbinates (Figure 12), Septum (Figure 13), and Frame (Figure 14). In particular, the frame was the last module that was designed since it was obtained by subtracting the other two modules from the entire nasal cavity with the *Boolean Difference* tool.

3.2.1. Turbinates Module

The Nasal Cavity group contains two sets of turbinates: upper, middle, and inferior, respectively. Upper turbinates are the smallest and are located in the narrowest zone of ETA, which is typically not involved in the procedure. Therefore, for the sake of simplicity and manufacturability, only middle and inferior turbinates were included in this module, while upper turbinates became part of the frame. Accordingly, both left and right turbinates were isolated from the entire nasal cavity using the *Plane Cut* tool, Figure 12. In particular, a prismatic shape was used at the interface with the frame (Figures 12 and 14b) to facilitate the design, the fabrication, and the final assembly phases. In fact, simple geometries increase the success rate when using the *Boolean Difference* tool, which was necessary in the design of the Frame module.

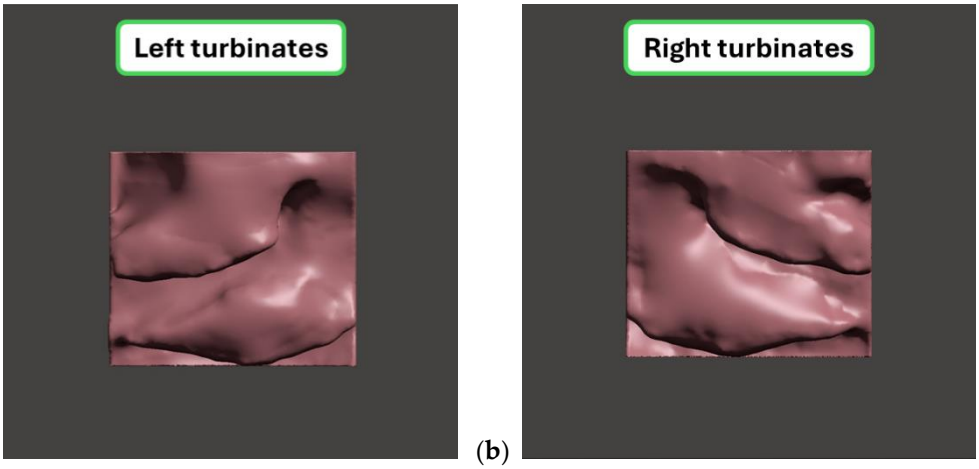

(**a**) (**b**)

Figure 12. Turbinates modules. The middle and lower turbinates of (**a**) the left and (**b**) the right sides.

3.2.2. Nasal Septum Module

The nasal septum module was designed similarly to the turbinate modules. It was isolated using the *Plane Cut* tool (Figure 13) obtaining two prismatic interfaces, upper and lower. The module includes the part of the septum within the nasal cavities, while the outer part remains in the external ethmoid bone of the Face group (Figure 6). This design choice is because the internal posterior portion of the septum may be cut to make room near the sphenoid sinus. On the contrary, the outer nasal septum is not cut. Accordingly, the internal nasal septum must be a disposable part of the model. (Table 1). Moreover, the Face group is a single-cast part, and it should allow the insertion of the septum within. This would require a core that is more complicated to be designed and assembled/disassembled with the ethmoid bone during the casting process. Moreover, the ethmoid bone has a low thickness. Therefore, it is more difficult, if not unfeasible, to design an interlocking geometry to mount and hold in place the septum. Given these considerations, the adoption of a unique septum module that is shared by the Nasal Cavity and Face groups would be an unnecessary complication.

Figure 13. Nasal septum module. The square-section parts on the top and the bottom were designed to facilitate the fabrication of the module and its insertion in the frame.

3.2.3. Frame Module

The frame is a box that holds turbinates and septum modules. Moreover, it connects and holds in place the Nasal Cavity group with the Face and Skull Base groups. The frame

was designed by subtracting the geometry of turbinates using the *Boolean Difference* tool (Figure 12) and the septum modules (Figure 13) from the nasal cavity model (Figure 11e). The dimensional geometrical accuracy of the FFF 3D printing process (approximately 0.2 to 0.5 mm) was considered in the design of the Frame module. In particular, to facilitate the insertion of turbinates and nasal septum modules, a wider interlocking geometry was designed. It was conducted by temporarily expanding the volume of the modules using the *Transform* tool under the *Edit* menu to offset their surface. Accordingly, a larger volume was removed, and a nominal allowance of 0.3 mm along each main direction was designed in the interlocking zones. Finally, two holes were designed with the *Boolean Difference* tool using two cylinders (as with the face module) on both sides of the frame to hold connecting plugs (Figure 14a). Figure 14b shows the frame with the turbinates and nasal septum modules inserted.

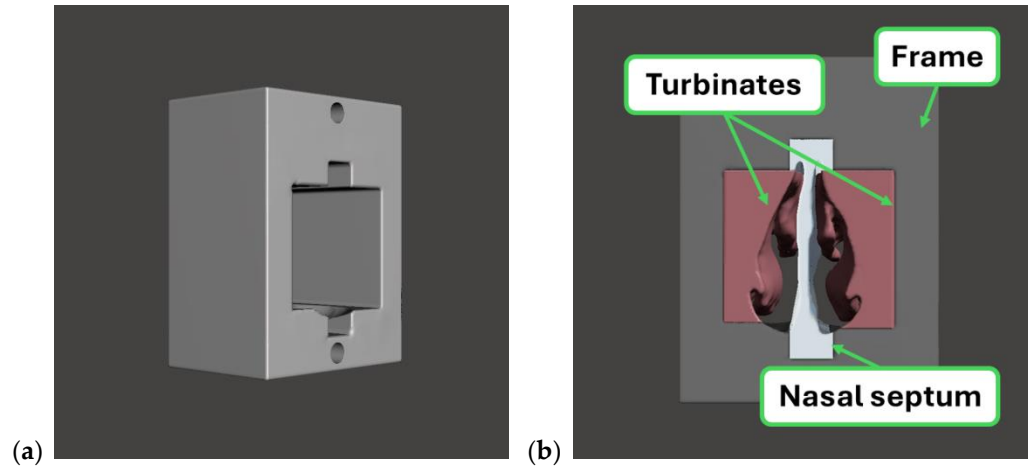

Figure 14. The frame module. The frame (**a**) and the frame with the turbinates and nasal septum module inserted (**b**).

3.3. Skull Base Group

The Skull Base group is composed of the sphenoid bone module and the arachnoid membrane together with the system to emulate the cranial pressure of the cerebrospinal fluid (CSF). The sphenoid bone is partially drilled during the surgical procedure to expose the pituitary tumor. Therefore, the sphenoid was subdivided into two parts, one disposable (upper sphenoid bone) and one reusable (lower sphenoid bone). Moreover, it was adapted to be mounted with screws. The rest, i.e., the arachnoid and the system containing the CSF, is part of further research focused on the implementation of sensors on the ETA model to provide real-time feedback during simulations. Its main characteristics are described below, and more details are reported in our previous work [63].

3.3.1. Sphenoid Bone

The sphenoid bone (Figure 3a) was cut into two halves using the *Plane Cut* tool, namely, the upper and lower sphenoid bone. The upper half (Figure 15a) contains the sella turcica and is the disposable part since it is drilled during the ETA simulation. The lower half (Figure 15b) was kept as a support of the upper sphenoid bone. Moreover, two flanges were added to each half using the *Boolean Union* tool for the assembly with the frame (Figures 4 and 15c).

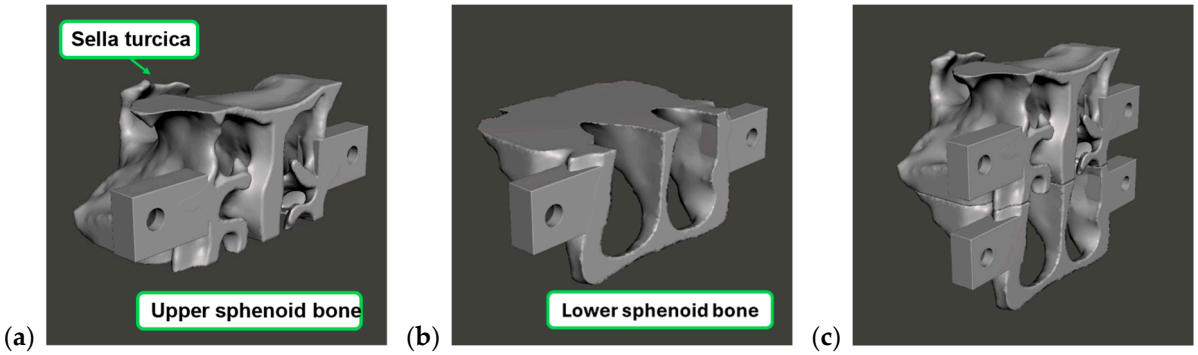

Figure 15. Sphenoid bone module. (**a**) Upper sphenoid bone with the sella turcica and (**b**) lower sphenoid bone. (**a**) The two modules are coupled (**c**). Each half is equipped with two flanges to mount them on the frame module.

3.3.2. Arachnoid and Cranial Pressure

The addition of the arachnoid membrane is in development (Figure 16). Based on our previous studies, we decided to implement a sensor-based non-anatomical module to replicate two features that are not present in the current commercial products. The first feature replicates the fall of the suprasellar arachnoid within the sellar region. This is meant to train the surgeon to move the arachnoid membrane without breaking it and subsequently causing a CSF leakage, which is one of the most common complications related to surgery [4]. The second feature provides the surgeon with feedback on the force applied to the membrane together with a measure of the CSF leak risk.

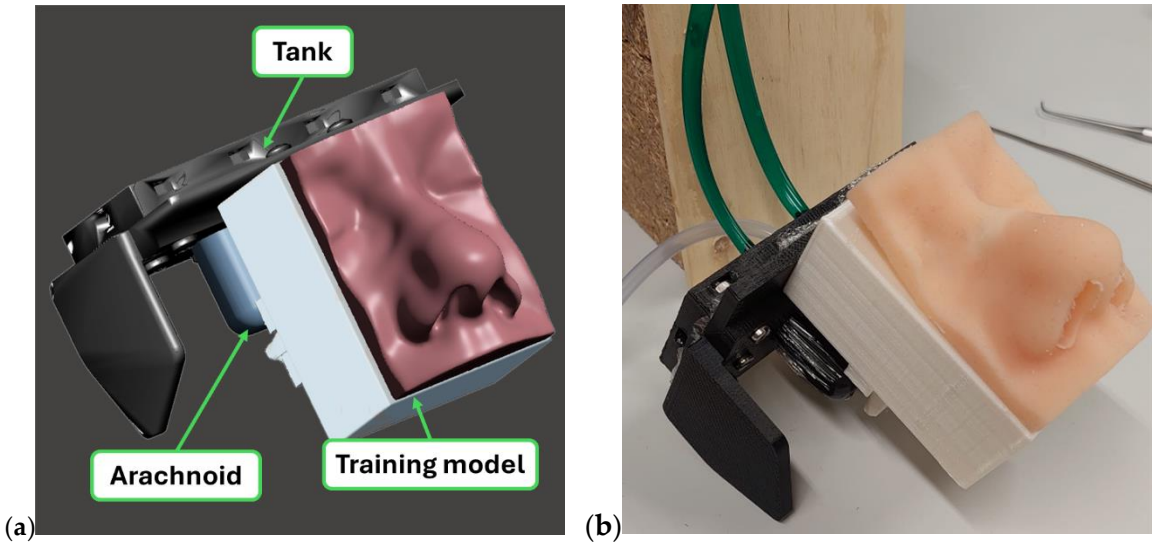

Figure 16. The training model is equipped with the sensor-based tank, i.e., the system that simulates the fall of the arachnoid within the sella turcica. (**a**) The CAD model, (**b**) the system mounted.

The module consists of a tank filled with distilled water to mimic the CSF. The system is sealed on one side with a polymeric food film that reproduces the arachnoid, as suggested by the literature [33,34]. In particular, intracranial pressure expands the arachnoid, which falls inside the sella turcica thus filling the space left after tumor removal [1]. Furthermore, the group is also equipped with a pressure sensor that can measure the force exerted by surgeons when interacting with the arachnoid, whose preliminary design and tests are reported in our previous study [63].

4. Rapid Manufacturing

The model fabrication involved two prototyping processes, direct 3D printing (modules made of PLA and TPU, Figure 17) and rapid casting processes (silicone modules, Figure 18).

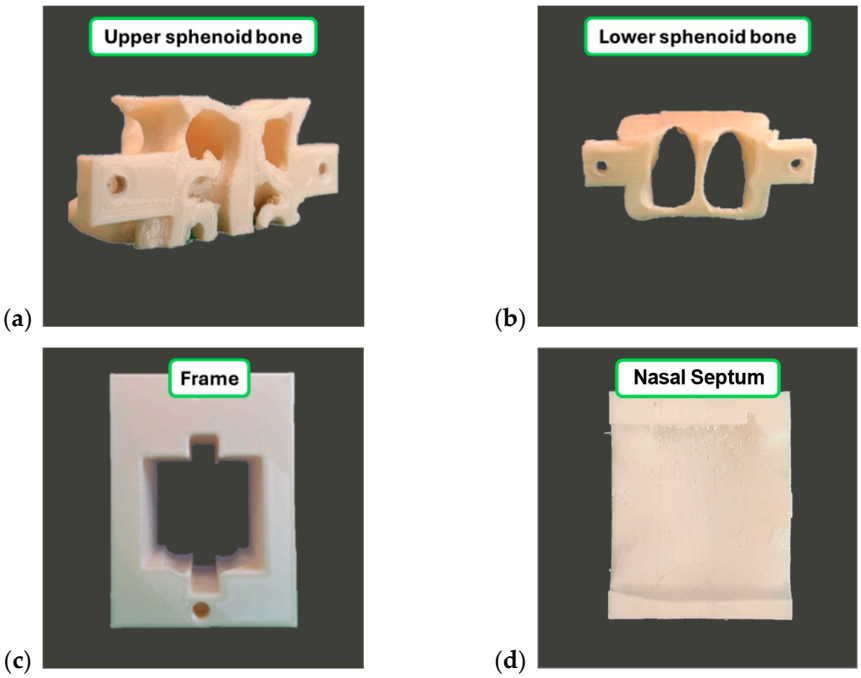

Figure 17. Direct 3D-printed modules: both the sphenoid bone module and the frame were 3D-printed in Pearl-White PLA (**a**–**c**), while the nasal septum was 3D-printed in TPU (**d**).

The Ultimaker 3 extended printer equipped with an AA04 nozzle and 2.85 mm filament was used to print modules in both Pearl-White PLA and TPU 95A and rigid tools in Pearl-White PLA using a layer height of 0.1 mm. The infill density was 20% for PLA and 100% for TPU. Pouring molds were made of the two components of the silicone Mold Star™ 15 SLOW (Smooth-On, Inc., Macungie, PA, USA), which has a Shore A hardness of 15 and a pot life of 50 min. As already mentioned, casted parts were made of the two components of the silicone Dragon Skin™ 30. To replicate skin color, the Light Flesh™ pigment (Smooth-On, Inc., USA) was added to the Dragon Skin™ silicone. Furthermore, Ease Release™ 205 (Mann Release Technology, Macungie, PA, USA) was used as a release agent. The silicones were degassed before pouring using a 90% vacuum chamber.

In rapid casting, cores and possible inserts are initially printed (Figure 18a). The silicone used for the molds is prepared and degassed to remove the air entrapped during pouring and mixing (Figure 18b). Then, the pattern with landmarks is temporarily fixed on a clay substrate inside a box, and a releasing agent is applied on the surfaces that will be in contact with the silicone (Figure 18c) during the pouring of the first half of the mold (Figure 18d). Once the silicone is cured, the clay is removed. The half mold and pattern are turned upside down, the lateral embankment and pattern of the pouring channel (made of clay) are added, and, finally, the release agent is applied (Figure 18e). The second half mold is then poured onto the first one (Figure 18f). After solidification, the pattern is removed, the core and inserts are positioned, vents may be cut on the parting plane (if required), and the releasing agent is applied (Figure 18g) to obtain the mold (Figure 18h). To cast the part, silicone is prepared, degassed (Figure 18i), and poured (Figure 18j). If vents are used, the mold should be tilted to facilitate air release. Once solidified, the core is removed from the part, and the pouring channel is cut (Figure 18k) to obtain the final part (Figure 18l).

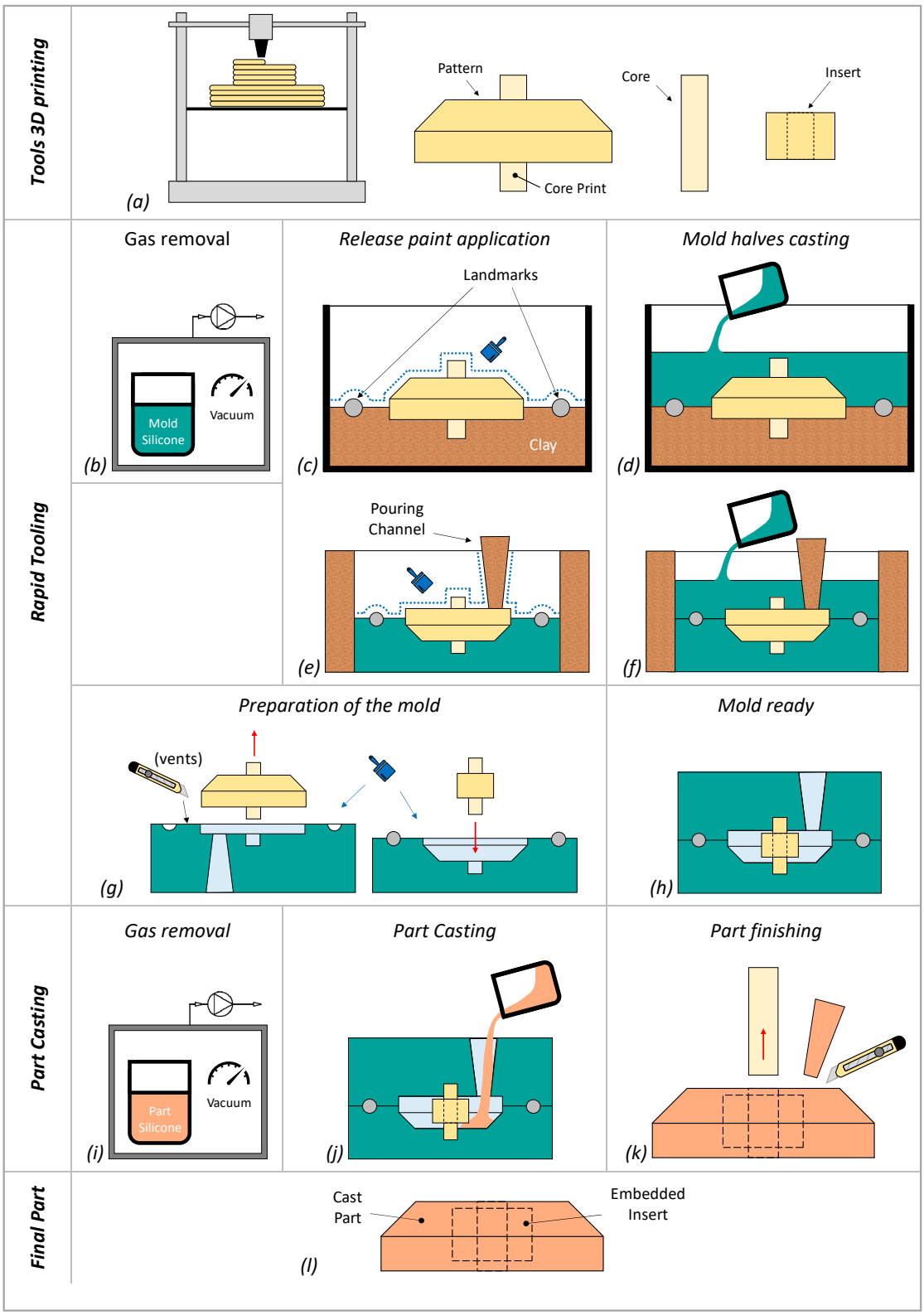

Figure 18. The procedure of the rapid casting of silicone parts. (**a**) Tools 3D printing, (**b**–**h**) rapid tooling steps, (**i**,**j**,**k**) part casting steps and (**l**) final cast part with insert and passing through cavity.

Figure 19 shows some steps of the rapid casting of the Face module. Figure 19a shows the pattern positioned on clay (Figure 19b, as shown in the illustration in Figure 18c) and the resulting mold half (Figure 19c, as shown in the illustration in Figure 18d). Figure 19c shows the mold with the nostril cores and ethmoid bone in place (as shown in Figure 18g).

Figure 19d reports the cast face group with the embedded ethmoid bone insert (as shown in Figure 18l). Similar results were achieved in the rapid casting of the turbinates (Figure 19e).

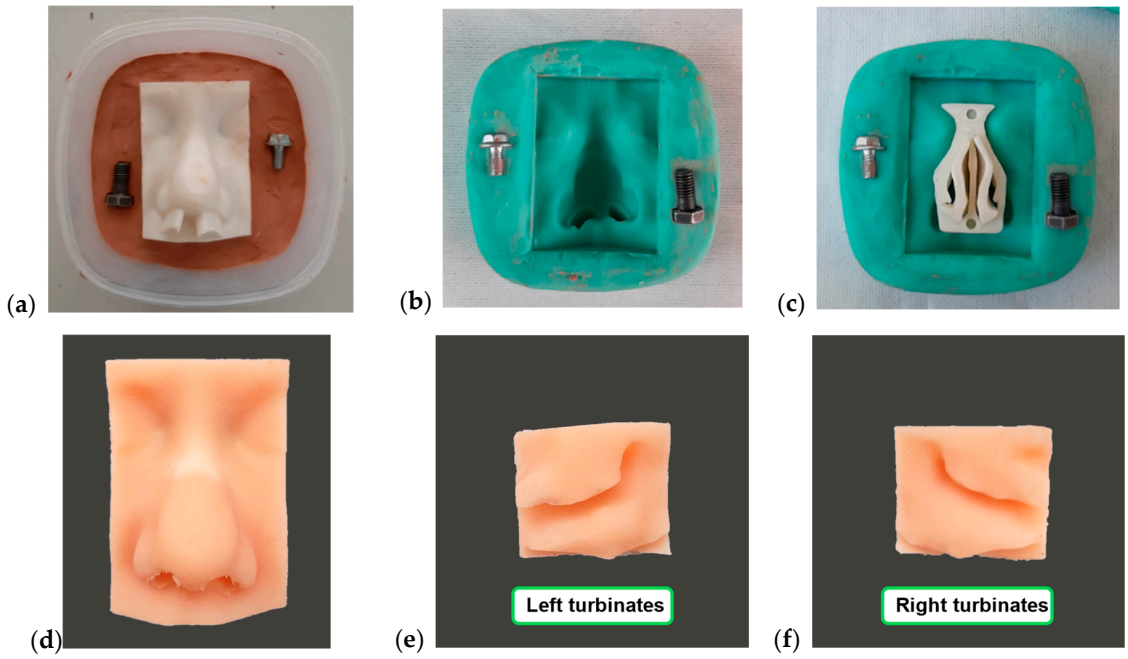

Figure 19. Main steps of the rapid casting of the Face group and the nostril modules. (**a**) Pattern positioned before casing the (**b**) mold silicone. After curing, (**c**) Ethmoid bone insert and nostril cores are positioned in the silicone mold. Part silicone is casted and the parts are extracted: (**d**) Face group and (**e**,**f**) turbinates.

Figure 20 shows a comparison between the CAD model of the training model (Figure 20a) and the final training model (Figure 20b).

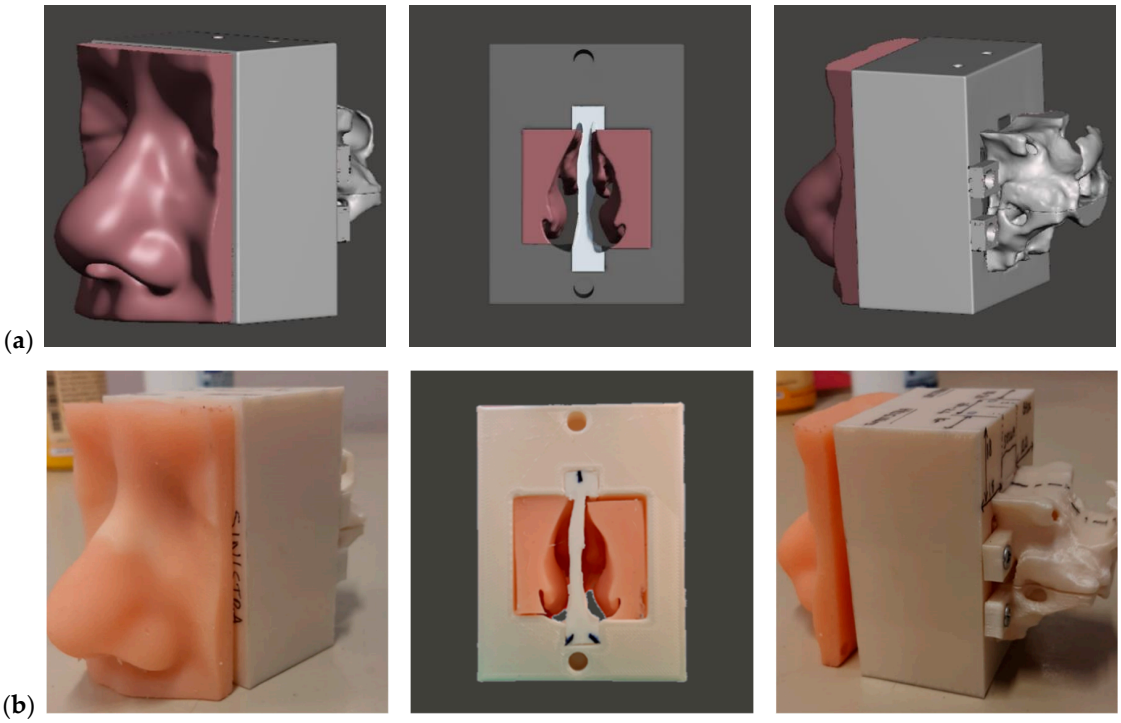

Figure 20. The CT-based anatomical training model. CAD (**a**) and assembled model (**b**).

5. Training Model Validation and Cost Assessment

The presented solution was assessed from two points of view, surgical and economical. In particular, the model was directly tested by expert neurosurgeons who provided their feedback, which was used for the first validation of the anatomy and materials. Moreover, an estimation of the design and manufacturing costs was made.

5.1. Anatomy and Materials

A real surgical procedure was simulated using an endoscope, surgical curette, drill, and forceps (Figure 21). Figure 21a shows the endoscopic view when passing through the left side of the nasal cavity while the spatula is moving the turbinates to the side. Figure 21b shows the dissection of the sphenoid bone to expose the sellar region and reach the pituitary tumor. The dissected sphenoid bone disassembled after the test is reported in Figure 21c. During the test, an attempt was made to drill, and scissors were used to cut the septum (Figure 21d).

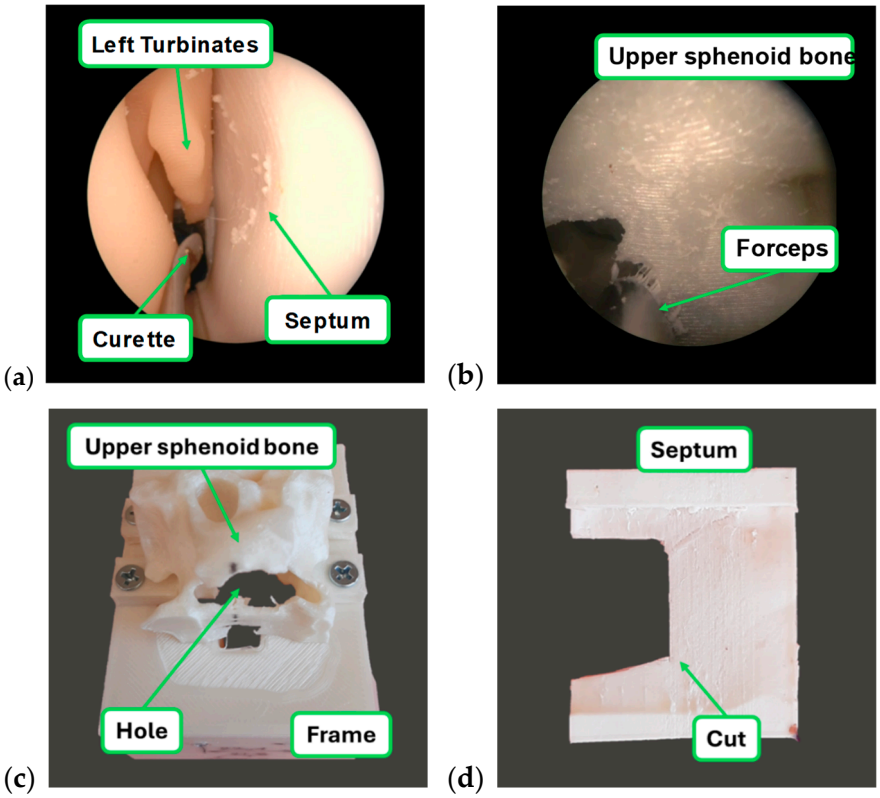

Figure 21. Surgical tests to validate the training model. Endoscopic view of the nasal cavity (**a**) and upper sphenoid bone (**b**). Disposable parts after the surgical tests (**c**,**d**).

The surgeon's feedback indicated was as follows:

- The patient's anatomy is accurately replicated, although the thickness of the sphenoid bone and the nasal septum is slightly greater than expected.
- The response of PLA during the dissection of the sphenoid bone was good. The removal with the forceps and drill is similar to reality, even though a "chewy" behavior is present. Preliminary wetting of the model surfaces is preferable to prevent chip sticking to the tip of the drill, which that may occasionally occur.
- The flexural strength of the TPU used for the nasal septum is comparable to real tissue. Drilling was not applicable since the material mostly melts instead of chipping due to high friction with the drilling tool. Scissor cutting was applicable, even though the

excessive thickness of the septum required a high cutting force. This aspect can be solved by lightening its thickness.

- The flexural strength of silicone is comparable to real tissue. Instead, its spring-back is too high, causing the turbinates to move out of place instead of remaining fixed. To address this issue, a plastic element, such as a metal wire, could be incorporated into the silicone to achieve the desired functionality.

5.2. Cost Estimation

Design and manufacturing costs were estimated to evaluate the training model from an economic point of view and to compare it with the price of commercial ones. Costs were evaluated on the basis of materials and time required by the design and fabrication of the prototype (Table 6). In particular, the design of the parts required approximately 30 h of direct CAD editing. Moreover, printing material and time were estimated using the slicing software. Furthermore, the purchasing cost of silicone was used in the costing procedure. The unit cost of the manual tasks was assumed to be 22.7 EUR/h based on the experience, and the unit costs of PLA and TPU were 0.048 EUR/g and 0.088 EUR/g based on the market prices, respectively.

Table 6. Design and manufacturing cost assessment of the training model.

		Material		***Process time***		***Cost***		
		g	***EUR/g***	***h***	***EUR/h***	***Material***	***Time***	***Sum***
CAD design	*STL editing*	-	-	30	22.7	-	681 EUR	**681 EUR**
Direct AM	*Part 3D printing—PLA*	172	0.048	16.5	0.14	8.3 EUR	2.3 EUR	**35 EUR**
	Part 3D printing—TPU	10	0.088	2.5	0.14	0.9 EUR	0.4 EUR	
	Post-process	-	-	1	22.7	-	23 EUR	
Casting	*Silicone casting*	(lump sum)		3	22.7	170 EUR	68 EUR	**258 EUR**
	Silicone curing	-	-	4	-	-	-	
	Spare parts	(lump sum)		-	-	20 EUR	-	
Assembly	*Assembly*	-	-	1	22.7	-	23 EUR	**23 EUR**
			Total	**58**		199 EUR	797 EUR	**996 EUR**

Results in Table 6 show that the overall cost of the prototype is approximately 1000 EUR, and a lead time of 58 h is required. Most of the cost is due to CAD design time, which covers 68% of the final cost. The fabrication process of a replica (direct printing, rapid casting, and assembly) requires 28 h and costs 315 EUR. Considering that the cost of the prototype is slightly overestimated (patterns and cores are reusable) along with scale factors that reduce the lead time and cost of commercial products, the proposed solution is comparable, if not competitive, in cost compared to products on the market (Table 2, silicone-casted models, 200 USD).

6. Discussion

During the development of the design and manufacturing procedures of the ETA model, general aspects and comments were drawn.

The steps that lead to the prototype of the ETA model are summarized in Table 7 and discussed as follows.

Table 7. Summary and guidelines for the design and fabrication of the ETA prototype.

Step	**Details**		
Material and Process Selection	***Tissue***	***Process Design***	***Notes***
	Bone	Material: PLA Process: FFF	-
	Soft tissue (skin, mucosa)	Material: Silicone Process: Rapid casting	Flexible molds made of silicone
	Cartilage (Nasal Septum)	Material: TPU 95A Process: FFF	-
CAD design	***Focus***	***Editing procedure***	***Tools sequence (Meshmixer)***
	Mesh fix	Preliminary operations (isolated parts, close STL)	*Analysis* > *Inspector* > *Auto Repair*
		Local editing (small artifacts removal)	*Sculp*
		Internal holes removal	*Select* * (on surfaces to preserve) > *Modify* > *Invert* > *Discard*
	Part design (modules and molds)	Crop	*Edit* > *Plane Cut*
		Interlocking with allowances	*Object Browser* > *Select object * (module)* *Edit* > *Transform—Size X/Y/Z* *Object Browser* > *Select objects * (modules and other objects)* *Boolean Difference*
	Core Design	Hole surface selection	*Select* * (on hole edge borders) > *Smooth Boundaries* > *Modify* > *Create FaceGroup* *Object Browser* > *Duplicate* *Delete* (the mesh outside the hole)
		Volume from surface	*Select* * (on hole surface) > *Edit* > *Flip Normals* *Analysis* > *Inspector* > *Auto Repair (Flat Fill)*
		Print core design	*Select* * (on core end surfaces) > *Edit* > *Extrude (Normal direction)*
		Removal of (eventual) interferences	*Object Browser* > *Select objects ** *Edit* > *Boolean Difference*
	Objects Union (Pattern)	Join (module + core prints)	*Object Browser* > *Select objects ** *Edit* > *Combine* *Object Browser* > *Select (new) object ** *Edit* > *Make Solid*

* Keep the elements or objects selected.

- *Materials and process selection*. Materials were chosen according to the literature to enhance the mimicking of real tissue. Then, the more suitable additive manufacturing processes were chosen. For bone and cartilage (made of PLA and TPU, respectively), direct 3D printing was adopted, while rapid casting was selected for soft tissues (made of silicone).
- *CAD design*. Four main design phases were identified: mesh fixing and the design of modules, cores, and patterns (or, generally, object union). They are generalized and reported together with the sequence of tools and commands in Figure 18 and Table 7.

Furthermore, the following aspects of the procedure emerged during its implementation.

- *Forward procedure.* The steps of the procedure are straightforward, which reduces the product development time and enhances the anatomical accuracy. In fact, editing an STL file generally leads to geometrical approximations; therefore, fewer setbacks accumulate less geometrical approximations in the part.
- *CAD skills*. The procedure strongly depends on human technical skills and experience, especially in the CAD design and casting phases. In particular, the success in editing STL mesh files deeply depends on both the quality of the mesh and the sequence of commands. The mesh can be improved (smoothing, remeshing), but this may significantly reduce the precision and accuracy of the part. Hence, the experience of the designer is fundamental. Concerning the correct sequence of commands for successful editing, the paper provides robust guidelines that help the design process.
- *Manual silicone casting*. The manual procedure requires additional lead time compared to the direct fabrication of the parts. Conversely, their mechanical properties are limited by the commercial feedstock materials. Moreover, printing rubber-like materials to emulate soft tissues may require high-performance technologies (such as MultiJet or PoliJet). SLA may represent an exception to this generalization, although it is subject to the material limitations mentioned above. Conversely, manual silicone casting provides a larger capability of replicating soft tissues' mechanical properties. Moreover, it is generally a low-cost solution compared to direct printing, as shown by the price of commercial products (Table 2).

Overall, the following general comments can be outlined on the model developed.

- *Validation.* The proposed procedure led to an accurate replication of the surgical operation. In particular, the overall anatomy, bone "drillability", and the flexibility of cartilage, mucosa, and skin are well simulated.
- *Improvements.* Some anatomical details should be improved (thickness of the sphenoid bone and nasal septum). Moreover, a wetting system could reduce the risk of the PLA melting during drilling and enhance the aesthetic result. Finally, the spring-back of turbinates needs to be removed.
- *Advantages of the model*. The modular design, together with casting silicone, makes the model highly customizable in anatomy and materials. Therefore, it is possible to emulate a specific surgical case on the basis of the surgeon's requests.
- *Fabrication time and cost.* Most of the development costs of the model were given by the CAD design phase. A replica of the prototype approximately costs 300 EUR and can be produced in less than 2 working days, values that may be lower in a mature product. These estimations confirm the economic soundness of the product when compared with competitors (Tables 2 and 3).
- *Enhancements to the market*. The model can be equipped with an instrumented module that can emulate the effects of intracranial pressure on the arachnoid. Moreover, it provides direct feedback to the surgeon, who can measure her/his skill or learning curve.

7. Conclusions

This work describes the full procedure developed to fabricate a modular model for ETA surgery training. The procedure starts with the patient's CT data, which was converted into an STL model and edited with the open-source software Meshmixer v3.5.474. In particular, the anatomy of the skull base, nasal cavity, and patient's face was designed. Then, their components were fabricated using additive manufacturing technology. In particular, FFF 3D printing and rapid casting processes were involved. Once assembled, the model was tested by neurosurgeons, which provided a preliminary validation of the model. Moreover,

the cost and time assessments demonstrated the consistency of the product as a competitor in the market.

During the development of the model, a general procedure to design the parts of the model and their additive manufacturing or rapid casting processes was outlined. Aspects such as the materials suitable to replicate the behavior of bone, cartilage, and mucosa were investigated. Moreover, the working procedure of a silicone-cast part with an embedded insert and passing-through cavities was provided.

Overall, the model received positive feedback for anatomical fidelity and material behavior. Moreover, suggestions for the improvement of the model were provided. In particular, a reduction in wall thickness in some areas (skull base and nasal septum) and the reduction in silicone spring-back (turbinates) were suggested. Moreover, the use of a more drillable material to replace the TPU would be preferable.

The next prototypes of the model will focus on the suggested aspects. The introduction of other anatomical details that can raise the training complexity (such as the presence of optic nerves or the carotid artery) will be considered. Moreover, a bleeding system will be introduced to provide a more vivid and realistic experience.

Author Contributions: G.S. (Investigation, Writing—original draft preparation), A.F. (Conceptualization, Methodology, Writing—review and editing, Supervision), F.D. (Conceptualization, Validation, Supervision), M.S. (Conceptualization, Supervision). All authors have read and agreed to the published version of the manuscript.

Funding: This research received no external funding.

Institutional Review Board Statement: The study was conducted in accordance with the Declaration of Helsinki, and the protocol was approved by the Ethics Committee of Brescia (NP 3464) on 7 May 2019.

Informed Consent Statement: Informed consent was obtained from all subjects involved in the study.

Data Availability Statement: Dataset available on request from the authors.

Conflicts of Interest: The authors declare no conflict of interest.

References

1. Santona, G.; Madoglio, A.; Mattavelli, D.; Rigante, M.; Ferrari, M.; Lauretti, L.; Mattogno, P.; Parrilla, C.; De Bonis, P.; Galli, J.; et al. Training Models and Simulators for Endoscopic Transsphenoidal Surgery: A Systematic Review. *Neurosurg. Rev.* **2023**, *46*, 248. [CrossRef]
2. Berhouma, M.; Baidya, N.B.; Ismaïl, A.A.; Zhang, J.; Ammirati, M. Shortening the Learning Curve in Endoscopic Endonasal Skull Base Surgery: A Reproducible Polymer Tumor Model for the Trans-Sphenoidal Trans-Tubercular Approach to Retro-Infundibular Tumors. *Clin. Neurol. Neurosurg.* **2013**, *115*, 1635–1641. [CrossRef]
3. Alomari, A.; Alsarraj, M.; Alqarni, S. The Learning Curve in Endoscopic Transsphenoidal Skull-Base Surgery: A Systematic Review. *BMC Surg.* **2024**, *24*, 135. [CrossRef] [PubMed]
4. Ahn, Y.; Lee, S.; Shin, D.-W. Learning Curve for Endoscopic Transsphenoidal Surgery: A Systematic Review and Meta-Analysis. *World Neurosurg.* **2024**, *181*, 116–124. [CrossRef]
5. Salmi, M. Additive Manufacturing Processes in Medical Applications. *Materials* **2021**, *14*, 191. [CrossRef] [PubMed]
6. Fiorentino, A.; Piazza, C.; Ceretti, E. Anti-Migration Enhanced Tracheal Stent Design, Rapid Manufacturing and Experimental Tests. *Rapid Prototyp. J.* **2016**, *22*, 178–188. [CrossRef]
7. Colpani, A.; Fiorentino, A.; Ceretti, E. 3D Printing for Health & Wealth: Fabrication of Custom-Made Medical Devices through Additive Manufacturing. *AIP Conf. Proc.* **2018**, *1960*, 140006.
8. Zhuo, C.; Lei, L.; Yulin, Z.; Wentao, L.; Shuangxia, W.; Chao, W.; Yaqian, Z.; Shuman, H.; Dong, D. Creation and Validation of Three-Dimensional Printed Models for Basic Nasal Endoscopic Training. *Int. Forum Allergy Rhinol.* **2019**, *9*, 695–701. [CrossRef] [PubMed]
9. Bartikian, M.; Ferreira, A.; Gonçalves-Ferreira, A.; Neto, L.L. 3D Printing Anatomical Models of Head Bones. *Surg. Radiol. Anat.* **2019**, *41*, 1205–1209. [CrossRef] [PubMed]

10. Naftulin, J.S.; Kimchi, E.Y.; Cash, S.S. Streamlined, Inexpensive 3D Printing of the Brain and Skull. *PLoS ONE* **2015**, *10*, e0136198. [CrossRef] [PubMed]
11. Singhvi, M.S.; Zinjarde, S.S.; Gokhale, D.V. Polylactic Acid: Synthesis and Biomedical Applications. *J. Appl. Microbiol.* **2019**, *127*, 1612–1626. [CrossRef]
12. Mitsouras, D.; Liacouras, P.; Imanzadeh, A.; Giannopoulos, A.A.; Cai, T.; Kumamaru, K.K.; George, E.; Wake, N.; Caterson, E.J.; Pomahac, B.; et al. Medical 3D Printing for the Radiologist. *Radiographics* **2015**, *35*, 1965–1988. [CrossRef]
13. Riva, L.; Pagani, R.; Fiorentino, A.; Borboni, A. Additive Manufacturing of PLA to Mimic the Thrust Force of Mandibular Bone during Drilling. *Procedia CIRP* **2022**, *110*, 199–202. [CrossRef]
14. Dąbrowska, A.K.; Rotaru, G.-M.; Derler, S.; Spano, F.; Camenzind, M.; Annaheim, S.; Stämpfli, R.; Schmid, M.; Rossi, R.M. Materials Used to Simulate Physical Properties of Human Skin. *Skin Res. Technol.* **2016**, *22*, 3–14. [CrossRef]
15. Shen, Z.; Xie, Y.; Shang, X.; Xiong, G.; Chen, S.; Yao, Y.; Pan, Z.; Pan, H.; Dong, X.; Li, Y.; et al. The Manufacturing Procedure of 3D Printed Models for Endoscopic Endonasal Transsphenoidal Pituitary Surgery. *Technol. Health Care* **2020**, *28*, 131–150. [CrossRef] [PubMed]
16. Liacouras, P.; Garnes, J.; Roman, N.; Petrich, A.; Grant, G.T. Designing and Manufacturing an Auricular Prosthesis Using Computed Tomography, 3-Dimensional Photographic Imaging, and Additive Manufacturing: A Clinical Report. *J. Prosthet. Dent.* **2011**, *105*, 78–82. [CrossRef] [PubMed]
17. Lamouche, G.; Kennedy, B.F.; Kennedy, K.M.; Bisaillon, C.-E.; Curatolo, A.; Campbell, G.; Pazos, V.; Sampson, D.D. Review of Tissue Simulating Phantoms with Controllable Optical, Mechanical and Structural Properties for Use in Optical Coherence Tomography. *Biomed. Opt. Express BOE* **2012**, *3*, 1381–1398. [CrossRef] [PubMed]
18. Kashapov, L.N.; Kashapov, N.F.; Kashapov, R.N.; Pashaev, B.Y. The Application of Additive Technologies in Creation a Medical Simulator-Trainer of the Human Head Operating Field. IOP Conf. *Ser. Mater. Sci. Eng.* **2016**, *134*, 012011. [CrossRef]
19. Masalha, M.A.; VanKoevering, K.K.; Latif, O.S.; Powell, A.R.; Zhang, A.; Hod, K.H.; Prevedello, D.M.; Carrau, R.L. Simulation of Cerebrospinal Fluid Leak Repair Using a 3-Dimensional Printed Model. *Am. J. Rhinol. Allergy* **2021**, *35*, 802–808. [CrossRef]
20. Colpani, A.; Fiorentino, A.; Ceretti, E. Feasibility Analysis and Characterization of an Extrusion-Based AM Process for a Two-Component and Biocompatible Silicone. *J. Manuf. Process.* **2020**, *49*, 116–125. [CrossRef]
21. Colpani, A.; Fiorentino, A.; Ceretti, E. Design and Fabrication of Customized Tracheal Stents by Additive Manufacturing. *Procedia Manuf.* **2020**, *47*, 1029–1035. [CrossRef]
22. Engel, D.C.; Ferrari, A.; Tasman, A.-J.; Schmid, R.; Schindel, R.; Haile, S.R.; Mariani, L.; Fournier, J.-Y. A Basic Model for Training of Microscopic and Endoscopic Transsphenoidal Pituitary Surgery: The Egghead. *Acta Neurochir.* **2015**, *157*, 1771–1777; discussion 1777. [CrossRef]
23. Ding, C.-Y.; Yi, X.-H.; Jiang, C.-Z.; Xu, H.; Yan, X.-R.; Zhang, Y.-L.; Kang, D.-Z.; Lin, Z.-Y. Development and Validation of a Multi-Color Model Using 3-Dimensional Printing Technology for Endoscopic Endonasal Surgical Training. *Am. J. Transl. Res.* **2019**, *11*, 1040–1048.
24. Oyama, K.; Ditzel Filho, L.F.S.; Muto, J.; de Souza, D.G.; Gun, R.; Otto, B.A.; Carrau, R.L.; Prevedello, D.M. Endoscopic Endonasal Cranial Base Surgery Simulation Using an Artificial Cranial Base Model Created by Selective Laser Sintering. *Neurosurg. Rev.* **2015**, *38*, 171–178; discussion 178. [CrossRef] [PubMed]
25. Suzuki, M.; Ogawa, Y.; Kawano, A.; Hagiwara, A.; Yamaguchi, H.; Ono, H. Rapid Prototyping of Temporal Bone for Surgical Training and Medical Education. *Acta Otolaryngol.* **2004**, *124*, 400–402. [CrossRef] [PubMed]
26. Mori, K.; Yamamoto, T.; Oyama, K.; Nakao, Y. Modification of Three-Dimensional Prototype Temporal Bone Model for Training in Skull-Base Surgery. *Neurosurg. Rev.* **2009**, *32*, 233–239. [CrossRef]
27. Hochman, J.B.; Kraut, J.; Kazmerik, K.; Unger, B.J. Generation of a 3D Printed Temporal Bone Model with Internal Fidelity and Validation of the Mechanical Construct. *Otolaryngol. Head. Neck Surg.* **2014**, *150*, 448–454. [CrossRef]
28. Hochman, J.B.; Rhodes, C.; Wong, D.; Kraut, J.; Pisa, J.; Unger, B. Comparison of Cadaveric and Isomorphic Three-Dimensional Printed Models in Temporal Bone Education. *Laryngoscope* **2015**, *125*, 2353–2357. [CrossRef]
29. Tai, B.L.; Kao, Y.-T.; Payne, N.; Zheng, Y.; Chen, L.; Shih, A.J. 3D Printed Composite for Simulating Thermal and Mechanical Responses of the Cortical Bone in Orthopaedic Surgery. *Med. Eng. Phys.* **2018**, *61*, 61–68. [CrossRef] [PubMed]
30. Bjellerup, M. Novel Method for Training Skin Flap Surgery: Polyurethane Foam Dressing Used as a Skin Equivalent. *Dermatol. Surg.* **2005**, *31*, 1107–1111. [CrossRef] [PubMed]
31. Singh, R.; Singh, R.; Sen, C.; Gautam, U.; Roy, S.; Suri, A. Mechanical Characterization and Standardization of Silicon Scalp and Dura Surrogates for Neurosurgical Simulation. *World Neurosurg.* **2023**, *169*, e197–e205. [CrossRef]
32. Wanibuchi, M.; Noshiro, S.; Sugino, T.; Akiyama, Y.; Mikami, T.; Iihoshi, S.; Miyata, K.; Komatsu, K.; Mikuni, N. Training for Skull Base Surgery with a Colored Temporal Bone Model Created by Three-Dimensional Printing Technology. *World Neurosurg.* **2016**, *91*, 66–72. [CrossRef]
33. Harada, N.; Kondo, K.; Miyazaki, C.; Nomoto, J.; Kitajima, S.; Nemoto, M.; Uekusa, H.; Harada, M.; Sugo, N. Modified Three-Dimensional Brain Model for Study of the Trans-Sylvian Approach. *Neurol. Med.-Chir.* **2011**, *51*, 567–571. [CrossRef]

34. Lin, J.; Zhou, Z.; Guan, J.; Zhu, Y.; Liu, Y.; Yang, Z.; Lin, B.; Jiang, Y.; Quan, X.; Ke, Y.; et al. Using Three-Dimensional Printing to Create Individualized Cranial Nerve Models for Skull Base Tumor Surgery. *World Neurosurg.* **2018**, *120*, e142–e152. [CrossRef]
35. Gragnaniello, C.; Nader, R.; van Doormaal, T.; Kamel, M.; Voormolen, E.H.J.; Lasio, G.; Aboud, E.; Regli, L.; Tulleken, C.A.F.; Al-Mefty, O. Skull Base Tumor Model. *J. Neurosurg.* **2010**, *113*, 1106–1111. [CrossRef] [PubMed]
36. Okuda, T.; Kataoka, K.; Kato, A. Training in Endoscopic Endonasal Transsphenoidal Surgery Using a Skull Model and Eggs. *Acta Neurochir.* **2010**, *152*, 1801–1804. [CrossRef]
37. Mashiko, T.; Konno, T.; Kaneko, N.; Watanabe, E. Training in Brain Retraction Using a Self-Made Three-Dimensional Model. *World Neurosurg.* **2015**, *84*, 585–590. [CrossRef]
38. Narayanan, V.; Narayanan, P.; Rajagopalan, R.; Karuppiah, R.; Rahman, Z.A.A.; Wormald, P.-J.; Van Hasselt, C.A.; Waran, V. Endoscopic Skull Base Training Using 3D Printed Models with Pre-Existing Pathology. *Eur. Arch. Otorhinolaryngol.* **2015**, *272*, 753–757. [CrossRef] [PubMed]
39. Zheng, J.-P.; Li, C.-Z.; Chen, G.-Q.; Song, G.-D.; Zhang, Y.-Z. Three-Dimensional Printed Skull Base Simulation for Transnasal Endoscopic Surgical Training. *World Neurosurg.* **2018**, *111*, e773–e782. [CrossRef]
40. Zheng, J.-P.; Li, C.-Z.; Chen, G.-Q. Multimaterial and Multicolor 3D-Printed Model in Training of Transnasal Endoscopic Surgery for Pituitary Adenoma. *Neurosurg. Focus.* **2019**, *47*, E21. [CrossRef] [PubMed]
41. London, N.R.; Rangel, G.G.; VanKoevering, K.; Zhang, A.; Powell, A.R.; Prevedello, D.M.; Carrau, R.L.; Walz, P.C. Simulation of Pediatric Anterior Skull Base Anatomy Using a 3D Printed Model. *World Neurosurg.* **2021**, *147*, e405–e410. [CrossRef] [PubMed]
42. ProDelphus. Available online: https://www.gtsimulators.com/collections/pro-delphus (accessed on 31 January 2024).
43. SIMONT ENT AND SKULL BASE SIMULATOR—Youtube. Available online: https://www.youtube.com/watch?v=iUqcVprRXuk (accessed on 31 January 2024).
44. Neuroendoscopic Surgery Training Simulator—GTSimulators.Com. Available online: https://www.gtsimulators.com/products/neuroendoscopic-surgery-training-simulator-snt (accessed on 31 January 2024).
45. Japan Medical Company. Available online: https://japanmedicalcompany.co.jp/en (accessed on 31 January 2024).
46. 3D Printed Medical Anatomy Models from JAPAN | KEZLEX. Available online: https://www.kezlex.com/en/ (accessed on 31 January 2024).
47. 3D Printed Skull Base for Head Holder Model | A22 | KEZLEX. Available online: https://www.kezlex.com/en/products/skull/a22 (accessed on 31 January 2024).
48. 3D Printed Endoscopic for Pituitary Gland Model | A39 | KEZLEX. Available online: https://www.kezlex.com/en/products/skull/a39/ (accessed on 31 January 2024).
49. 3D Printed Internal Carotid Artery Injury ICAI Model Model | A43 | KEZLEX. Available online: https://www.kezlex.com/en/products/skull/a43/ (accessed on 31 January 2024).
50. Phacon—The Patients for Your Surgical Demonstration and Education. Available online: https://www.phacon.de/en/ (accessed on 31 January 2024).
51. Video Guide | PHACON Sinus Trainer—Youtube. Available online: https://www.youtube.com/watch?v=cBidMVMPpew (accessed on 31 January 2024).
52. [S-00007] PHACON Sinus Assistant—Phacon Available. Available online: https://phacon.de/en/shop/hno/s-00007-phacon-sinus-assistant/ (accessed on 31 January 2024).
53. [S-00005] PHACON Sinus Trainer—Phacon. Available online: https://phacon.de/en/shop/hno/s-00005-phacon-sinus-trainer/ (accessed on 31 January 2024).
54. Endoscopy—Getting Started | PHACON Sinus Assistant—Youtube. Available online: https://www.youtube.com/watch?v=Iy9QACSR6AY (accessed on 31 January 2024).
55. [SN-Ah] PHACON Sinus Patient "Meyer"—Pituitary Tumor—Phacon. Available online: https://phacon.de/en/shop/hno/sn-ab-phacon-sinus-patient-meyer/ (accessed on 31 January 2024).
56. The Evolution of Neurosurgery Learning | UpSurgeOn. Available online: https://www.upsurgeon.com/scientific-news/neurosurgery-evolution-origins-to-modern-innovations-part-i/ (accessed on 31 January 2024).
57. TNSBox—UpSurgeOn Store. Available online: https://store.upsurgeon.com/products/tnsbox/2023 (accessed on 31 January 2024).
58. Disposable Cavities—UpSurgeOn Store. Available online: https://store.upsurgeon.com/products/disposable-cavities/ (accessed on 31 January 2024).
59. TNS Box | Self-Training System for Endoscopic Pituitary Surgery—Youtube. Available online: https://www.youtube.com/watch?v=71-lGn5yIck (accessed on 31 January 2024).
60. UltiMaker PLA TDS. Available online: https://support.makerbot.com/s/article/1667410781972 (accessed on 31 January 2024).
61. UltiMaker TPU 95A TDS. Available online: https://support.makerbot.com/s/article/1667410781018 (accessed on 31 January 2024).
62. Download SDS and Technical Bulletins (TB/TDS). Available online: https://www.smooth-on.com/documents/?doc=all (accessed on 31 January 2024).

63. Santona, G.; Fapanni, T.; Fiorentino, A.; Doglietto, F.; Serpelloni, M. Preliminary Study of a Sensorized System for Real-Time Feedback for Arachnoid Collapse during Neurosurgical Training. In Proceedings of the 2023 IEEE International Workshop on Metrology for Industry 4.0 & IoT (MetroInd4.0&IoT), Brescia, Italy, 6–8 June 2023; pp. 233–238.
64. Okuda, T.; Yamashita, J.; Fujita, M.; Yoshioka, H.; Tasaki, T.; Kato, A. The Chicken Egg and Skull Model of Endoscopic Endonasal Transsphenoidal Surgery Improves Trainee Drilling Skills. *Acta Neurochir.* **2014**, *156*, 1403–1407. [CrossRef] [PubMed]
65. Wen, G.; Cong, Z.; Liu, K.; Tang, C.; Zhong, C.; Li, L.; Dai, X.; Ma, C. A Practical 3D Printed Simulator for Endoscopic Endonasal Transsphenoidal Surgery to Improve Basic Operational Skills. *Childs Nerv. Syst.* **2016**, *32*, 1109–1116. [CrossRef] [PubMed]
66. Gallet, P.; Rebois, J.; Nguyen, D.-T.; Jankowski, R.; Perez, M.; Rumeau, C. Simulation-Based Training in Endoscopic Endonasal Surgery: Assessment of the Cyrano Simulator. *Eur. Ann. Otorhinolaryngol. Head. Neck Dis.* **2021**, *138*, 29–34. [CrossRef]
67. Santona, G.; Fapanni, T.; Fiorentino, A.; Doglietto, F.; Serpelloni, M. Preliminary Study on a 3D Printed Sensorized Probe to Characterize Pituitary Adenoma Hardness. In Proceedings of the 2023 IEEE International Workshop on Metrology for Industry 4.0 & IoT (MetroInd4.0&IoT), Brescia, Italy, 6–8 June 2023; p. 253.
68. Santona, G.; Fiorentino, A.; Doglietto, F.; Serpelloni, M. A Novel 3D Printed Sensorized Surgical Instrument to Characterize Pituitary Adenoma: Development and Initial Validation. In Proceedings of the 2024 IEEE International Workshop on Metrology for Industry 4.0 & IoT (MetroInd4.0 & IoT), Firenze, Italy, 29–31 May 2024; pp. 7–11.